Fiber Singular Optics

Alexander V. Volyar

National Taurida V. Vernandsky University. Physical Department.4, Yaltinskaya str. Simferopol, Crimea, 95007 Ukraine, e-mail: volyar@ccssu.crimea.ua

Received 15.02.2002

Abstract

The present review is devoted to the optical vortex behavior both in free space and optical fibers. The processes of the vortex transformations in perturbed optical fibers are analyzed on the base of the operator of the spin – orbit interaction in order to forecast the possible ways of manufacturing the vortex preserving fibers and their applications in supersensitive optical devices.

Key words: optical vortex, singular beam.

PACS: 42.81.-i,42.81.Dp, 67.57.Fg

Contents:

I. Historical Introduction

Diversity of natural wave phenomena as a rule is associated with events of birth, death and evolution of optical singularities. In particularly, the rainbow – the most amazing optical effect as it had been showed by Airy in 1830 s manifests itself as a result of the ray's contact with some imaginary surface - a caustic (see, for instance, the work [1] and references to it). At the ray's

caustic, the field intensity is infinitely large. Airy in his wave theory had revealed that there is finite value of intensity due to the light diffraction. At present Berry and Nye have recognized and given the mathematical substantiation (see, for instance, the work [2] and references to it) to the fact that the caustic has a fine wave structure and consists of the constellation of phase singularities – the wavefront dislocations.

The other astonishing optical phenomenon also discovered first by Airy [3] is the forming of anomalous rings near the lens focal plane. A detailed consideration of this effect, first realized by Ignatovskii in 1919 [4], had brought to light an interesting fact – an energy flow near the anomalous ring can have opposite propagation direction in free space with respect to the initial one. It seemed that the fundamental theoretical study of this phenomenon developed by Richards and Wolf [5] in 1959, Wolf [6] and Boivin, Dow, Wolf [7] in 1967 had totally concluded this topic. However, Carter in 1973 [8] revealed on the base of computer simulation that the rings could appear and disappear due to very slight perturbations of the light beam. Subsequently, the experimental developments by Karman et. al. [9] and the theoretical study by Berry [10], Nye [11], Volyar et. al. [12,13] showed that the anomalous rings or the ring wavefront dislocations accompany propagation of any nonparaxial laser beam. Besides variations of the beam's parameters cause dislocation reactions – chains of birth and death events of wavefront singularities. More recently Soskin, Vasnetsov and Pas'ko [14] have represented the main properties of the ring and edge dislocations as a spatial motion of the transverse optical vortices – the elementary cells bearing phase singularities and as an example of axis optical vortices (pure screw dislocations) Soskin and Vasnetsov [22] experimentally and theoretically displayed a partial recovery of the vortex properties after a larger portion of a singular beam had been truncated by any obstacle. In fact, the wave vortices are inherent to any wave phenomena both of classic and quantum nature, from Aharonov – Bohm effect [15,16] to oil bubbles on a frying pan, being the brightest example of self-organization effects, and from the Dirac monopole [17] to the giant universe eddies as a consequence of the big bang. As a rule, the vortex propagation and its transformation are characterized by Berry's phase [18] – the most lucid demonstration of the topological nature of the vortices. The vortex prehistory emerges due to an evolution of this phase that in turn can also prophesy a subsequent vortex behavior.

A great deal of monographs and review papers have been published on the optical vortices problem by the end of 20^{th} century, among them the comprehensive work by Nye on the fine structure of optical singularities [2]; the "catastrophe" analysis of optical phenomena by Wright [19], some important aspects of optical vortices by Vasnetsov and Staliunas [20]; the optical vortex solitons in nonlinear media by Kivshar and Pelinovsky [21], principles of singular optics [22] by Soskin and Vasnetsov. The important property of the optical vortices to carry over the angular momentum in free space was elucidated in detail by Allen, Pedgett, Babiker [23] and Barnet, Allen [42].

We would like to emphasize that the branch of physical and quantum optics studying the evolution of optical vortices and their derivation in various optical systems has acquired the name "Singular Optics" after M. Soskin's suggestion in 1999 [24]. Now this new discipline embraces a great deal of linear and nonlinear unusual optical phenomena including the processes inside laser cavity [25], subwavelength dislocation reactions in evanescent waves [10-13], singular fiber optics [26,27], computer – generated holography [28,29] and many others.

In the given paper we shall restrict our review to singular fiber optics. The aim of our paper is to briefly elucidate the main problems of singular optics of free space or homogeneous

isotropic media in order to discuss the most arduous topic of vortex behavior in guiding nonhomogeneous media.

II. Optical Vortices in Free Space

As a rule, the optical vortices cannot exist in free space. They are born and annihilated either inside a laser cavity [30] due to special introcavity gadgets or at the expense of diffraction processes on computer generated holograms [20,31], optical wedges [32] and other optical obstacles. Nevertheless, the main properties of a vortex generated by a laser or some way else are simpler to study as fast as it propagates through free space.

II.1 Ring Edge Dislocations

Any light scattering process somehow or other is connected with birth and annihilation events of phase singularities – wavefront dislocations [33]. However, a lifetime or lifelength of a given singularity is characterized by a kind of a medium inhomogeneity. Some dislocations may disappear near the optical obstacle but others together with the light beam propagate rather far. In the given section we consider a special type of singularities appearing and disappearing not far from an optical system enough to give birth to them. As early as the 19th century Airy drew attention [3] to the strange bright and dark rings forming in the vicinity of the focal plane of a microscope. Afterwards these patterns, called the anomalous Airy's rings, were considered by Wolf et. al. [5,6,7] in detail, but they were interpreted as the ring edge wavefront dislocations [9.10,11] only at the end of the 20th century. These phase singularities are born near a focal plane due to the light diffraction of a circular pupil of a microobjective and fast annihilated far from it. It is interesting to note that the ring dislocations are formed in nonparaxial Gaussian beams if one takes into account only plane waves with the real values of wave vectors cutting off evanescent waves [8]. In this case the anomalous rings are the result of the interference of the paraxial Gaussian beam and the diffracted part of the evanescent field [10]. At the same time, the ring dislocations also exist in the untruncated nonparaxial light beam near its waist [12,13, 34]. The fact is that the evanescent waves appear at the flexure vicinity of the light beam in free space [35], and it is the result of their interference that creates the ring edge wavefront dislocations. Let us consider this problem in detail [36].

The solutions of the scalar Kirchhof's equation:

$$\left(\nabla^2 + k^2\right)\Psi(x,y,z) = 0\,, \qquad (2.1)$$

(Ψ is the wave function, k is the wavenumber in free space) is symmetrically relative to the x, y, z coordinates while the light beam has a singled-out z-direction. This difficulty can be overcome if one introduces the complex-valued distance R with the z-coordinate assuming imaginary values [37]:

$$R = \sqrt{x^2 + y^2 + \left(z + iz_0\right)^2}\,, \qquad (2.2)$$

where $z_0 = k\rho^2/2$ is the Rayleigh length, ρ is the waist radius at $z = 0$. In this case the solution of eq.(1) for the light beams has the form:

$$\Psi(x,y,z) = \frac{1}{k^2}\left(\frac{x+iy}{R}\right)^l P_m^{(l)}(\cos\theta) j_m(kR)\,, \quad (2.3)$$

where $j_m(kR)$ is a spherical m-th order Bessel function of the first kind, $P_m^{(l)}(\cos\theta)$ is an associated Legendre polynomial, $\cos\vartheta = \left(z + iz_0\right)/R$. The solution (2.3) represents both nonparaxial and paraxial light beams. In order to see it one demands to hold true the following inequality: $kz_0 >> 1$, $r = \sqrt{x^2 + y^2} << z_0$.

Then $R \approx \left(z + iz_0\right)\left(1 + \dfrac{r^2}{2\left(z + iz_0\right)^2}\right)$ and the solution (2.3) is transformed for $m = 0$ into the well-known paraxial wave function [38]:

$$\Psi \propto \frac{1}{\sigma(z)}\left(\frac{x+iy}{\sigma(z)}\right)^{l} * \exp\left(-\frac{r^2}{\rho^2\sigma(z)}\right)\exp(ikz), \quad (2.4)$$

where $\sigma(z)=1+iz/z_0$. The transition from eq.(2.3) to the paraxial form for high-order light beams is more involved (see, for instance, [34,39]) since it is fulfilled within a narrow range of axial lengths near or far from a focal plane.

At the same time, the ring dislocations are positioned far from the optical axis where $r > z_0$ at a focal plane $z=0$. Indeed, the Fig.1a,b shows the calculated picture of the intensity distribution of the paraxial and nonparaxial lowest order ($l=m=0$) light beam.

The primary energy flow located near the optical axis is spanned with alternated dark and bright rings so that the ring's radii are larger than the Rayleigh length $r > z_0$. The location of the dark rings is [33]:

$$\mathrm{Re}[\Psi(x,y,z)]=0,\ \mathrm{Im}[\Psi(x,y,z)]=0. \quad (2.5)$$

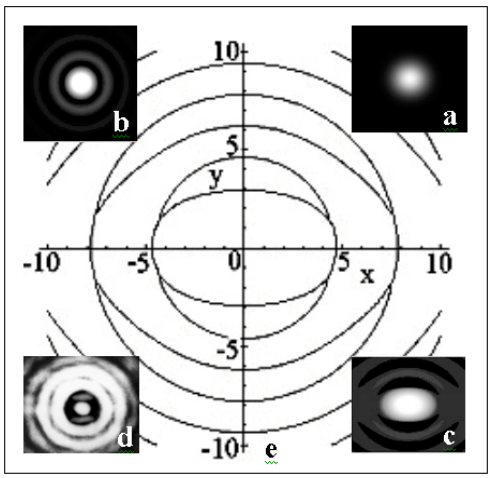

Fig.1 Fundamental mode beam $l=m=0$, $kz_0=1$: (a) the paraxial, (b) scalar nonparaxial and (c) the vector nonparaxial intensity distribution; (d) the photograph of the focal spot after the $90^{\times}$ microobjective and (e) the singular lines $P_z(x,y,0)=0$ of the y-polarized nonparaxial beam.

It means that the wavefront dislocation manifests itself at such places only where the real and imaginary parts of the wave function simultaneously vanish. Each of the above equations represents a surface in a space. The intersection of these surfaces makes up the space trajectory of the wavefront dislocation. In our case from eq.(2.3) we obtain the following expression: $j_0(kR)=\frac{\sin(kR)}{kR}=0$ which leads to:

$$x_m^2+y_m^2=z_0^2+\frac{m\pi}{k^2},\ z=0. \quad (2.7)$$

This equation characterizes the circumference family situated on the waist plane with the center at the optical axis.

Fig.2a depicts the typical pattern of the constant phase lines for a single dislocation on the *x-z* plane. Each phase line starts from an upper singular point and comes to the end at the lower one. Generally speaking the wave dislocation can be defined in terms of an integral around a circuit that contains within an isolated dislocation line [33]:

$$\oint d\Phi = 2\kappa l\pi, \quad (2.8)$$

where the integer l is the winding number or the topological charge and $\kappa=\pm1$ is its sign. In our case the dislocation propagates along a

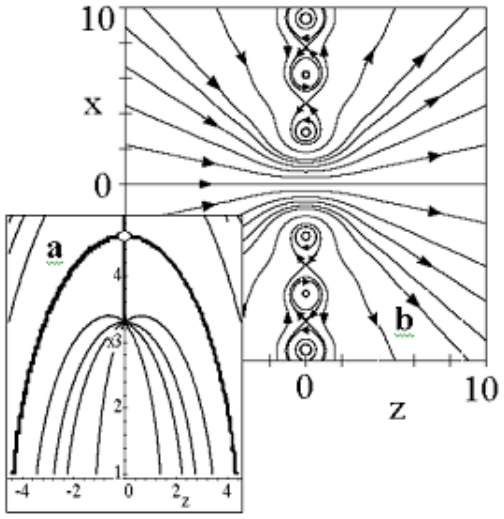

Fig.2 The equal phase lines (a) and Poynting vector trajectories (b) of the lowest-orde $l=m=0$, $kz_0=1$ nonparaxial light beam.

closed curve and the sign of its charge depends on the observer position [40].

In order to find the trajectories along which the energy flow propagates it is necessary to make use of the following expression [3]: $\vec{P} \propto |\Psi|^2 \nabla\Phi$, where $\vec{P}$ is the Poynting vector, Φ is the total phase of the wave function Ψ, while the directional vector of the energy flow is $\nabla\Phi / |\nabla\Phi|$. In our case the total phase is

$$\tan\Phi = 1/\tan(a\cos\phi)\tanh(a\sin\phi), \qquad (2.9)$$

where $a = \sqrt[4]{\left(r^2 + z^2 - z_0^2\right)^2 + 4z^2 z_0^2}$, $\phi = \frac{1}{2}\arctan\left(\frac{z}{r - z_0}\right) - \frac{1}{2}\arctan\left(\frac{z}{r + z_0}\right)$. In the vicinity of the dislocation point one finds: $\tan\Phi \approx a\varphi / \sin(a)$. Due to the shift of coordinates origin to the point r_m (see eq.(2.7)) : $r = r_m + \xi$, (ξ is the displacement relative to the r_m point) the expression (2.9) is transformed into $\Phi_m \approx \sqrt{\frac{z_0}{2a_m}}\frac{z}{\xi}$, $a_m = r_m - z_0$. The components of the Poynting vector are $P_z \propto 1/\xi$, $P_\xi \propto -z/\xi^2$. The trajectories of the energy flow can be found from the equation: $\frac{d\xi}{P_\xi} = \frac{dz}{P_z}$. Then the energy flow is transmitted near the dislocation points along the closed curves: $x^2 + y^2 = const$. Fig.2b illustrates the more exact computer calculation of the Poynting vector trajectories. The energy circulation is divided from the main flow by the separatrix line passing through the saddle point S marked on Fig.2a with a white circle.

The determination of the ring thickness is a detached problem. The fact is that we cannot determine the ring sizes from eq. (2.8) because it gives the zeros of the wave function but not the energy flow. The ring thickness can be found from the requirement of vanishing of the vector Poynting z-component: $P_z(x, y, 0) \propto e_x h_y^* - e_y h_x^* = 0$. The use of the expression $\vec{P} \propto |\Psi|^2 \nabla\Phi$ for the nonparaxial case is not correct.

To define the electric and magnetic field components we shall consider the wave function $\Psi = \sin(kR)/kR$ as the field potential and take advantage of the expressions [12]:

$$\begin{aligned} \mathbf{e} &= \nabla\times\nabla\times(\hat{\mathbf{n}}\Psi_1) - ik\nabla\times(\mathbf{n}\Psi_2) \\ \mathbf{h} &= -\sqrt{\varepsilon}\,\nabla\times\nabla\times(\mathbf{n}\Psi_2) - i\varepsilon k\nabla\times(\mathbf{n}\Psi_1) \end{aligned}, \qquad (2.10)$$

where $\mathbf{n}$ is the basic vector. The choice of the potentials $\{\Psi_1, \Psi_2\}$ may be confined within two cases: $\{\Psi, 0\}$ and $\{0, \Psi\}$. While the analysis of the fields has been discussed in detail in the works [11,12,36] we cite here the main results in the form of the distinctive curves. Fig.1e depicts the intensity distribution of the linearly polarized light beam at the waist plane. The beam form experiences some deformation along the direction of the electrical vector. Together with it the singularity lines are also subjected to some distortions. The typical singular lines deformation illustrated by Fig.1 points out the essential *polarization-dependent structure reconstruction*. Fist of all, it is necessary to remember that these singular lines are formed by the z-component of the Poynting vector $P_z(x, y, 0) = 0$ and therefore only one branch is consistent with the requirement: $\Psi(x, y, 0) = 0$. Secondly, the distance between two neighboring lines is equal to the ring thickness. However, this thickness changes along the ring in contrast to the consequences from the scalar approach. In the interval between the two lines the Poynting vector has the opposite direction relative to the initial one as it is represented on the Fig.2b. But the two singular lines collapse in the direction secant to the optical axis and perpendicular to the electrical vector. Thus the energy flow circulation at these places degenerates into the *cuspidal point* (the *cusp* on the current line) is located on the singular curve [11]. Estimations give the mean thickness of the ring up to $0.3\,\mu m$ at the waist plane $z = 0$ and about $0.8\,\mu m$ along the longitudinal direction.

Presented above the whirl of the energy flow and phase lines near the edge dislocations have enabled Berry [1] to compare this process with a vortex on the surface of slowly flowing water in a river. Soskin and Vasnetsov have called that process the *transverse optical vortex* [22]. Indeed, the energy circulation around the ring dislocations of the nonparaxial light beam conforms to the set of the *toroidal optical vortices* of an irregular form suspended at the focal plane. Any slight perturbation of the beam tears away these vortices from the maternal, dwelling forcing them to die and to be born anew being transmitted together with the light flow.

II.2 Pure Screw Dislocations

The exact solutions of the Maxwell's equations also contain the fields carrying over the second kind wavefront dislocations, which play an important role in the optical science. Being first revealed in scalar fields by Nye and Berry [33] and adopted by them as the pure screw dislocations, these field defects became the genuine matrix of the whole singular optics.

Let us consider the wave solution (2.4) of the scalar wave equation (2.1) in the paraxial approximation: $kz_0 >> 1$, $r << z_0$. This field has a wavefront surface in the form:

$$\Phi(r,\varphi,z) = kz - \frac{r^2}{2R(z)} + (l+1)\arctan\frac{z}{z_0} + l\varphi = const, \quad (2.11).$$

$$R(z) = \frac{z^2 + z_0^2}{z}$$

The basic part of the expression rewritten as $kz + l\varphi = const$ represents the straight helix with the *l*-branches. The path-tracing around the optical axis over the helix surface varies the wave phase to 2π. Therefore the distance between two neighbouring helix petals is equal to one wavelength λ.

Fig.3 shows the wavefront with the phase singularity. Because $\varphi = \arctan(y/x)$, the phase of the field is undefined on the optical axis: $x = y = 0$ but the field amplitude has vanished there as well. That singular point is called the pure screw dislocation by analogy with the screw defect in crystals [33] (in detail this analogy is considered in the work [22]). As it can be seen on Fig.3a, the phase is circulates around the optical axis. That seeming phase circulation is reflected both in the spiral interference pattern (depicted by Fig.3e or the fork-like interference pattern as it is shown on Fig 3d) and the real energy whirl. The Laguerre-Gaussian beam (2.4) can carry the angular momentum of light [23,41,42], and though the energy flows along the straight lines located on the surface of one sheet *hyperboloid*, its projections on the cross-section plane form the φ-component of the Poynting vector and, consequently, causes the *z*-component of the angular momentum [43]. These electromagnetic fields with pure screw dislocations are often called *axial optical vortices* [22] or simply *optical vortices*.

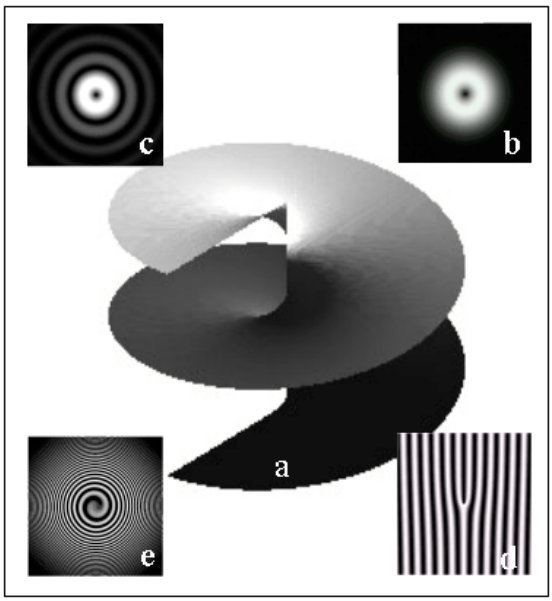

Fig. 3. Axial optical vortex: (a) the helical wavefront and intensity distributions in the paraxial Laguerre-Gaussian (b) and nonparaxial Legendre-Gaussian (c) beams. The interference pattern as a result of the sum of a paraxial beam bearing the optical vortex and a fundamental Gaussian beam transmitting at some angle (d) and along the same optical axis (e).

As a rule the nonparaxial light beam bears both the axial optical vortex and the toroidal optical vortices as it is depicted on Fig.3e.

II.3 Angular Momentum of Paraxial Optical Vortices

Light beams can carry both energy and momentum. As early as 1908 Poynting, showed by use of a mechanical analogy, that circularly polarized light should exert a torque per unit area on a quarter-wave birefringence plate, equal to k times the light energy per unit volume [23]. Naturally, rotation of a light field around the nodal line produces the vortex that bears an angular momentum. As the Poynting vector $\mathbf{P} = 1/2\,\mathrm{Re}\left(\mathbf{E}\times\mathbf{H}^{*}\right)$ is perpendicular to a wave front surface $\mathbf{P}\propto\nabla\Phi$ and the wave front surface of the vortex has a helicoidal shape, the cooperative effect of all Poynting vector lines produces an orbital angular momentum $L_z = i\left\langle\Psi\left|\partial/\partial\varphi\right|\Psi\right\rangle$ at a given cross-section of the beam. At the same time, since the light beam has always a certain polarization state, it must be possessed of the spin of angular momentum [44] $S_z = \left\langle\Psi\left|\hat{\boldsymbol{\sigma}}_z\right|\Psi\right\rangle$, where $\hat{\boldsymbol{\sigma}}_z$ is Pauli matrix. A total angular momentum represents the sum of the spin and orbit angular momenta: $M_z = L_z + S_z$ [23]. In order to show this, one considers the paraxial optical vortex in the form (2.4) and writes the Poynting vector components [43]:

$$P_r = \frac{r}{R(z)}\left|\Psi\right|^2,$$

$$P_\varphi = \frac{\omega l}{k r}\left|\Psi\right|^2 - \frac{\sigma l\omega}{2k}\frac{\partial\left|\Psi\right|^2}{\partial r},$$

$$P_z = \left|\Psi^2\right|.$$

The local angular momentum is $m_z = \left(\mathbf{r}\times\mathbf{P}\right)_z/c^2 = r\,P_\varphi$ while the total angular momentum is defined as $M_z = \int_S m_z dS$. Then one obtains the important relationship:

$$\frac{M_z}{c\int_S P_z dS} = \frac{l+\sigma}{\omega},$$

describing the angular momentum per one photon. This expression points out the fact that the total angular momentum is the superposition of the spin and orbital angular momenta: $M_z = \left\langle\Psi\left|\hat{l}_z + \hat{\sigma}_z\right|\Psi\right\rangle$.

Using the Poynting vector components one can make up the current lines of the energy flow: $dr/P_r = rd\varphi/P_\varphi$, $dr/P_r = dz/P_z$. The physical sense has only those current trajectories which satisfy the requirement of the light ray. In accordance with the quantum conception of the light rays [104,105], a light ray propagates along the trajectory where the wave function intensity is maximum $\left|\Psi(r_{\max})\right|^2_{\max}$. The trajectories of the energy flow is a set of straight lines lying on the hyperbolic surface: $\varphi = \kappa\arctan\left(z/z_0^{(\max)}\right)$, $\kappa = \pm 1$, $r^2 = \rho^2_{\max}\left[1+\left(z/z_0^{(\max)}\right)^2\right]$. Fig.4 illustrates the straight line trajectories pertaining to the set with the positive sign of the topological charge $\kappa = +1$. The opposite sign of the charge $\kappa = -1$ forms the mirrored line set. Not only straight lines but other trajectory forms (spirals, for instance as it was presented in the work [41,106]) that disagree with physical reality of the light propagation in free space.

At the same time, the Poynting vector in the region of the maximum energy flow is not dependant on the polarization state (in

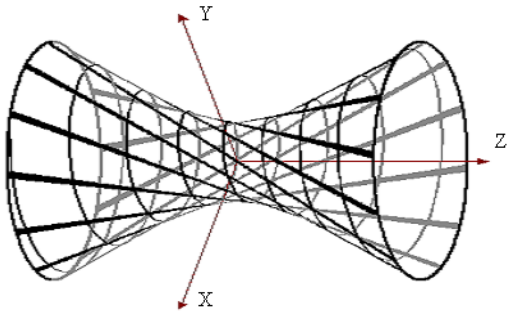

Fig.4. Schematic representation of the straight energy flow trajectories in an optical vortex with $\kappa = +1$.

particular, σ) but only on the topological charge $P_\varphi \propto \kappa l$. Since a paraxial vortex state $|\sigma, \kappa l\rangle$ in free space is characterized only by one number – a topological charge: $|\kappa l\rangle$ neglects its polarization that entirely conforms to the paraxial approximation of the Poynting vector [3].

Although the polarization state is the important characteristic of the paraxial beam, it cannot influence the forming of the vortex state.

II.4 Conversion of Optical Vortices

The singular beam with specific orbital angular momentum transmitted through some lens optical systems can be transformed into another beam with a different orbital angular momentum.

In particularly, the beam conversion often takes place at the expense of astigmatic optical elements [28, 45] causing the beam distortion and reproducing (or, vice versa, taking away) some share of the angular momentum. The most vivid instance of such mode conversion is the beam passing through the cylindrical lens [45].

The upper and lower fork-like interference patterns point out the topological charge inversion.

Let, for example, the superposition of two lower-order Hermite-Gaussian beams $(HG_{01} + HG_{10})$ with the degenerated edge dislocation directed at angle of 45^o relative to *x*-axis pass in series through two cylindrical lenses with the same focus length $f_1 = f_2 = f$ and positioned at the distance h from other. The astigmatic HG_{01} and HG_{10} mode beams gain different Gouy phases. The phase difference depends on both the focus length f and distance h between lenses. When the distance is $h = \sqrt{2} f$ the phase difference is $\pi/2$ and the Hermite-Gaussian beam changes into a Laguerre-Gaussian beam with $l = 1$ or the optical vortex. The sign (plus or minus) of the vortex topological charge is defined by the slope angle of the degenerated edge dislocation ($+45^o$ or -45^o). When the optical vortex with the topological charge $l = +1$ (Laguerre-Gaussian beam LG_{01}) passes through such a mode converter its topological charge changes into the opposite $l = -1$, provided that the distance between lenses is $h = 2f$.

Thus, the evolution of the paraxial singular beam in the astigmatic optical system is characterized by transformation of the angular momentum at the expense of differences in the Gouy phase respondent for the optical distortion. Conversion problems of high-order modes in the astigmatic systems are considered in the works [46,47].

However, a completely different type of situation occurs in propagation of a nonparaxial singular beam through free space. Now the state polarization, or in our case, the helicity σ takes part in the forming of the vortex state. This can be seen on the example of a combined nonparaxial mode beam consisting of even and

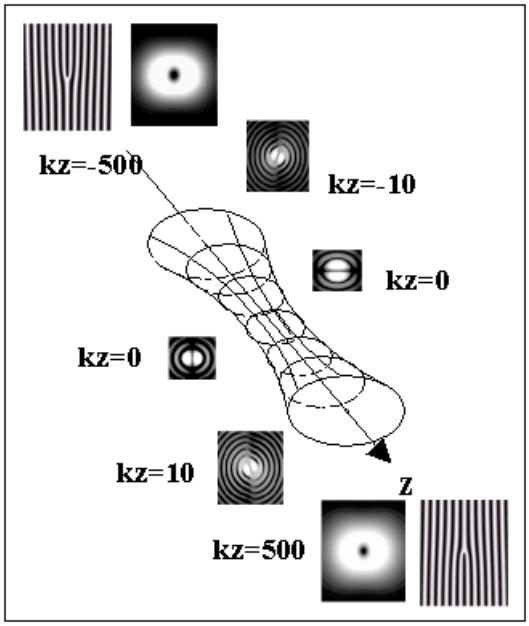

Fig.5. The self-conversion of the transverse and axial vortices and the self-inversion of the axial vortex topological charge in the combined even and odd circularly polarized nonparaxial singular beams with $l = 1$, $kz_0 = 3$.

odd vortices. The fact is that the even and odd nonparaxial beams have different *topological phases* [48] which have harsh variations as the beam approaches to its waist or moves off it.

The typical picture of the transformation of the beam structure shown on Fig.5 [12] elucidates the situation. The nonparaxial combined singular beam consists of two circularly polarized even and odd beams bearing the axial optical vortices with $l = +1$. Near the waist a linear pure edge dislocation (the transversal optical vortex) begins to be formed here which transforms into the axial vortex but with the topological charge $l = -1$ far from the focal plane. The change of the topological charge sign κ or the helicity σ far from the focal plane manifests itself as the rotation of the transverse vortex axis at the waist. The paraxial analog of this effect is studied in the work [49]. It should be expected that the *self-inversion* of the topological charge and the *self-conversion* between the transverse and axial vortices are the generic effects for most of nonparaxial wave processes.

II.5 Optical Vortex Generation

The problem of the creation of high-quality optical vortices is the most important one for practical work with singular beams. By the end of the century a whole series of original ways of the optical vortex generation, both by intro laser cavity and on the basis of the computer-generated holograms placed on the laser beam way (see, for example the works [20,22,30,50] and the references to them) was worked out. The most prevalent and convenient method of constructing vortex masks at present uses computer-generated holography [51-54], which has the advantages of rapid and inexpensive production, simple fabrication steps and adequate phase control. However, the energy-diffractive efficiency of this method is very low (1-5%). At the same time, recently, a completely unexpected high-energy-effective way of vortex creation has been revealed on the basis of the laser beam diffraction by an optical wedge [55-57].

Let us consider briefly this method in accordance with the work [58]. The light diffraction on the edge of the optical wedge positioned on the beam path, as it is shown on Fig.6, causes the formation of the optical vortex

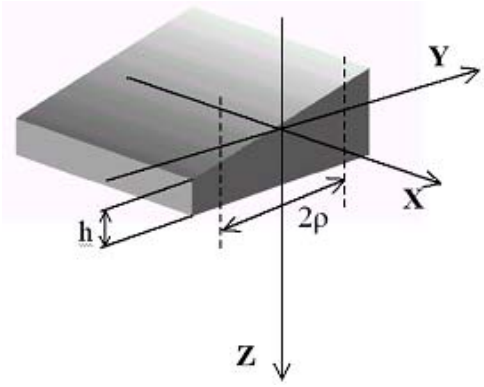

Fig.6. Schematic representation of the optical wedge

at the far field. One part of the beam passes through the wedge while the other propagates in free space. The calculation with the help of the diffractional Kirchhof's integral shows that the field far from the waist plane has the following form:

$$\Psi(x,y,z) = \frac{i\pi}{2k}\frac{z}{|\sigma|^2}\exp[-2i\Gamma]\exp\left[-\frac{x^2+y^2}{w^2}\right]\times$$
$$\left\{\exp\left[-iA\frac{k(Az-2y)}{2\sigma}\right]\exp(ikh)\,erfc\left[\frac{\sqrt{ik}\;x}{\sqrt{2z\sigma}}\right]+erfc\left[-\frac{\sqrt{ik}\;x}{\sqrt{2z\sigma}}\right]\right\} \quad (2.12),$$

where $A = (n_w - 1)tg\alpha$, $w^2 = \rho^2|\sigma(z)|^2$, $\Gamma = \arg[\sigma(z)] = arctg\frac{z}{z_0}$, h – the height of the mask substrate, α – the angle of the wedge. In general the equation (2.12) describes the vortex's lace illustrated by Fig.7c. The each

generic vortex of the lace is characterized with level lines of constant intensity. Near the vortex center the level lines gain an elliptic form. In order to estimate the line form one takes advantage of the *stereographic projection* properties. The wave function (2.12) at the vicinity of the *generic vortex* center can be rewritten as

$$\begin{aligned}\Psi' &\propto (x'\ y')\frac{1}{z}\vec{\Im} \\ &=(x'\ y')\frac{1}{z}\begin{pmatrix}\Im_x\\ \Im_y\end{pmatrix} \\ &=(x'y')\frac{1}{z}\begin{pmatrix}c\sqrt{kz_0}\left[bB+i(1-aB)\right]\\ kz_0AB(a+ib)\end{pmatrix},\end{aligned} \qquad (2.13)$$

where $B=\exp\left(A^2kz_0\right)$, $\exp(ikh)=a+ib$, $c=\sqrt{2/\pi}$. The column vector $\vec{\Im}$ similar to the Jones's vector in the polarization optics [61] enables us to make up the stereographic projection in the form:

$$L_0=1$$

$$L_1=\left|\Im_x\right|^2-\left|\Im_y\right|^2= =\frac{B^2\left(c^2-X^2\right)+c^2\left(1-2aB\right)}{B^2\left(c^2+X^2\right)+c^2\left(1-2aB\right)}$$

$$L_2=\Im_x\Im_y^*+\Im_x^*\Im_y= =\frac{2cbXB}{B^2\left(c^2+X^2\right)+c^2\left(1-2aB\right)}, \qquad (2.14)$$

$$L_3=i(\Im_x^*\Im_y-\Im_x\Im_y^*)= =\frac{2cXB(a-B)}{B^2\left(c^2+X^2\right)+c^2\left(1-2aB\right)}$$

$$X=\sqrt{kz_0}A$$

The ellipticity degree will be equal to the unity provided that $(c+X)\exp\left(-X^2\right)=c$, $a=\pm1, b=0$. The obtained conditions correspond to the circular form of the level lines. It means that if the height of the mask substrate is $h=m\lambda$, $m=1,2,3,...$ and $X=-0{,}8525$, that is the radius of the beam waist at the wedge plane is $\rho_{opt}=\left(0{,}8525\sqrt{2}\right)\frac{1}{(n-1)\,tg\alpha}\left(\frac{\lambda}{2}\right)$, then the *generic optical vortex* gains an ideal form (Fig.7a,b).

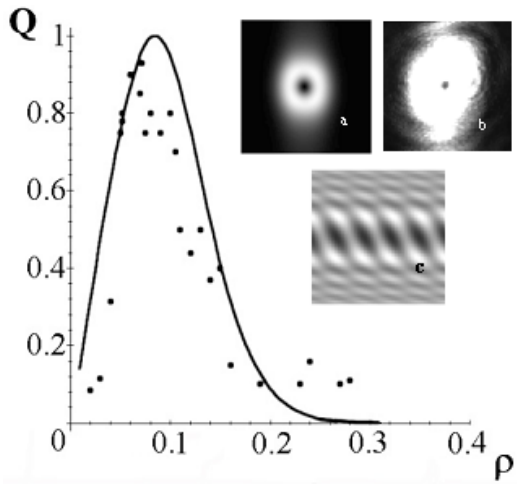

Fig.7. The experimental (the black points) and theoretical (the solid curve) results on the generic optical vortex: the dependency of the vortex ellipticity Q on the beam waist ρ (at the center); the intensity distributions of the wedge-generated optical vortex maximum ellipticity – (a) theory $Q_{\max}=1$, (b) experiment $Q_{\max}=0.93$, (c) the lace of the generic optical vortices; the wedge's angle $\alpha\approx2\cdot10^{-3}$ *rad* and its height $h\approx392{,}7\lambda$, $\lambda=0.6328\,\mu m$, $n=1{,}51$.

It should be noted that the *z*-component of the orbital angular momentum is calculated as $L_z=i\left\langle\Psi\left|\frac{\partial}{\partial\varphi}\right|\Psi\right\rangle$ is equal to $L_z=L_3$. In fact, we can experimentally measure the value of the orbital momentum of the generic optical vortex by means of measuring the ellipse semiaxes $\tilde{a}$ and $\tilde{b}$ since $\tan\chi=\tilde{b}/\tilde{a}$ and $\sin2\chi=S_3$. The cusp-like curve of the generic optical vortex ellipticity measured both experimentally and theoretically is illustrated by Fig.7 (at the center).

If the energy-effectiveness η of the generic optical vortex is estimated as the ratio of the total field intensity to the vortex intensity at the level 0.05, then the η value obtained

experimentally is 0.95 which is rather a good result for the constructing of technical devices on the base of optical vortices.

III. Fiber Optical Vortices

We find the first report on the vortical nature of fiber field radiation in the paper by Zel'dovich, Baranova and Mamaeyev [60] in which they theoretically and experimentally studied the fork-like interference structure of the scattering laser field, picking out the screw and edge phase dislocations. Later on Zel'dovich and others in the work [61] revealed the filtration method of a single pure screw dislocation. In 1996 Volyar and Fadeyeva (see, for instance, the works [62,63] and references to them) noticed the fact that the optical vortices are the form of the existence of guiding fiber modes and described their main properties. Volostnikov and others studied field evolution and singularities conversion in the liquid-wire parabolic waveguide in the paper [64]. The fine structure of singular beams scattered from dielectric stripe waveguides and other random-inhomogeneous media have been considered in the works [65,66].

Just as in free space the optical vortices in a fiber are characterized both by the topological charge l and helicity σ but here they are not independent. These physical values are connected with each other in a fiber inhomogeneous medium by means of the spin – orbit interaction [67,68]. It is this effect that determines the evolution peculiarities of the guiding vortices in the optical fibers [13]. For the first time this problem evoked by Zel'dovich and others in the works [69-71,101] has received further development in the work [72]. Using this method enables the authors of the papers [78,79] to bring to light the generic vortical processes in perturbed optical fibers and forecast the ways of the vortex preserving [80] and recovering [81] in complex fiber-optical systems.

Let us consider some aspects of the vortex transmitting through the single optical fibers.

III.1 Eigen Guided Vortices of Ideal Optical Fibers: Base Conception

Let the straight optical fiber have a refractive index of a core n_{co} and a clad n_{cl} so that $n_{co}^2 - n_{cl}^2 \approx 2n_{co}\Delta n$ and $\Delta n = n_{co} - n_{cl} > 0$. Such a fiber, typical for the optical region, is called the *weakly guiding fiber*. Further we shall use only such a type of fiber based on the approach by Snyder and Love [82].

III.1.1 Degenerated Case

Waves in inhomogeneous media are described by the vector wave equation:

$$\begin{aligned}&\nabla^2 \mathbf{E} - n^2(x,y,z)\frac{\partial^2 \mathbf{E}}{\partial t^2} \\ &+ \nabla\left[\mathbf{E}\cdot\nabla \ln n^2(x,y,z)\right]=0\end{aligned} \quad . \tag{3.1}$$

Since we shall consider only monochromatic waves $\mathbf{E} = \widetilde{\mathbf{E}}\exp(i\omega t)$ transmitted through a perfect straight optical fiber with a refractive index $n = n(x,y)$ where the *transmission invariance* is fulfilled: $\widetilde{\mathbf{E}} = \mathbf{e}(x,y)\exp(-i\beta z)$ (β is a propagation constant), the wave equation (3.1) for the transverse components $\mathbf{e}_t(x,y)$ can be rewritten in the form [82]:

$$\begin{aligned}&\left(\nabla_t^2 + n^2(x,y)\,k^2\right)\mathbf{e}_t \\ &+ \nabla_t\left(\mathbf{e}_t\cdot\nabla_t \ln n^2(x,y)\right) = \beta^2\mathbf{e}_t\end{aligned} \tag{3.2}$$

while the longitudinal component e_z is determined from the expression:

$$e_z \approx \frac{i}{k}\nabla_t \mathbf{e}_t \,. \tag{3.3}$$

Such approximation is quite justified for the weakly guided fibers: $n_{co} \approx n_{cl}$ with the refractive index $n^2(R) = n_{co}^2\left[1 - 2\Delta f(R)\right]$, $R = r/\rho$, ρ is fiber radius, $r^2 = x^2 + y^2$, $\Delta \approx (n_{co} - n_{cl})/n_{cl}$, $f(R)$ is a form of the refractive index profile.

In the null approximation we disregard the second term in eq.(3.2) and transform this

equation into:

$$\left(\nabla_t^2 + n^2(x,y)\,k^2\right)\tilde{\mathbf{e}}_t = \tilde{\beta}^2\tilde{\mathbf{e}}_t . \qquad (3.4)$$

The latter expression being the equation for eigenvalues $\tilde{\beta}^2$ of the operator $\hat{H}_0 = \nabla^2 + n^2(x,y)k^2$ presents the degenerate case. The degeneracy is lifted by the perturbation operator $\hat{H}_{\text{int}}$ as it will be shown later on, so that

$\tilde{\mathbf{e}}_t(x,y) \to \tilde{\mathbf{e}}_t(x,y) + \delta\mathbf{e}_t(x,y)$, $\tilde{\beta} \to \tilde{\beta} + \delta\beta$.

Nevertheless, the degenerate case enables us to calculate the degenerate "levels" of the propagation constant $\tilde{\beta}_{lm}$ and define the eigenfunction spectrum $\tilde{\mathbf{e}}_t$. The eigenfunction of the eq.(3.4) can be represented in the circular polarized basic $\hat{\mathbf{c}}^\sigma = \hat{\mathbf{x}} + i\sigma\hat{\mathbf{y}}$, where $\hat{\mathbf{x}}$ and $\hat{\mathbf{y}}$ are the unit vectors, in the form

$$\tilde{\mathbf{e}}_l^{(\kappa,\sigma)}(r,\varphi) = \hat{\mathbf{c}}^\sigma F_l(R)\exp(i\kappa l\varphi), \qquad (3.5)$$

where the radial function $F_l(R)$ is defined by the equation:

$$\left\{\frac{d^2}{dR^2} + \frac{1}{R}\frac{d}{dR} - \frac{l^2}{R^2} + \tilde{U}^2 - V^2 f(x,y)\right\}F_l = 0 , \qquad (3.6)$$

$V = k\rho n_{co}\sqrt{2\Delta}$ - the waveguide parameter, $\tilde{U}$ - the waveguide parameter of a core.

In our paper we shall mainly deal with step-index fibers: $f(R) = 0, 0 \le R < 1$ and $f(R) = 1, 1 < R < \infty$, though the results obtained can be extended for an arbitrary profile $f(R)$. The eigenvalues $\tilde{\beta}_{lm}$ are defined by the dispersion equation [82]:

$$\tilde{U}\frac{J_{l+1}(\tilde{U})}{J_l(U)} = \tilde{W}\frac{K_{l+1}(\tilde{W})}{K_l(\tilde{W})},$$

$$\tilde{\beta}^2 = \frac{1}{\rho}\left(\frac{V^2}{2\Delta} - \tilde{U}^2\right), \qquad (3.7)$$

where the eigenfunction factor $F_l(R)$ has a form:

$$F_l(R) = \frac{J_l(\tilde{U}R)}{J_l(\tilde{U})}, \quad 0 \le R < 1 \text{ and}$$

$$F_l(R) = \frac{K_{l;}(\tilde{W}R)}{K_l(\tilde{W})}, \quad 1 < R < \infty , \qquad (3.8)$$

$J_l(\xi)$ is a Bessel function of the first kind l- th order, $K_l(\xi)$ is the McDonald function, $\tilde{W}$ - is the waveguide parameter of a clad, $V^2 = \tilde{U}^2 + \tilde{W}^2$ and $l = 0,1,2...$.

The function $J_l(\xi)$ near the point $\xi = 0$ is $J_l(\xi) \propto \xi^l$, consequently, the expression (3.5) describes the fields bearing the axis optical vortices – the *guided vortices*. If one denotes the states in which the guided vortices can exist as $|\sigma, \kappa l\rangle\_(l > 0)$, we obtain the following four states: $|+1,+l\rangle$, $|-1,-l\rangle$, $|+1,-l\rangle$ and $|-1,+l\rangle$. The vortices with the same signs of the topological charge l and helicity σ: $|+1,+l\rangle$ and $|-1,-l\rangle$ are called the uniform circular polarized ones while the rest of the fields: $|+1,-l\rangle$ and $|-1,+l\rangle$ are called nonuniform because of the proper distribution of the angular momentum of their fields [27, 72].

In the degenerate case no properties of the guided vortices differ at all from those of the optical vortices in free space or a homogeneous medium [13] unless their phase velocities have intermittent values defined by eq. (3.7). It should be noted that any linear superposition of the four vortical states including linearly polarized vortices for the given topological charge l forms also the steady states propagating along the fiber without any decays as long as all these modes have the same propagation constant $\tilde{\beta}_l$.

III.1.2 Non-Degenerated Case: Spin – Orbit Interaction

The second term in the wave equation (3.2) has a higher order as compared with the other terms. Its contribution to the wave function (3.5) manifest itself as the polarization corrections $\delta\mathbf{e}_t(x,y)$ to the field $\tilde{\mathbf{e}}_t(x,y)$ and $\delta\beta$ to the propagation constant $\tilde{\beta}$. Although the value $\delta\beta$

is much smaller than $\widetilde{\beta}$: $\widetilde{\beta} >> \delta\beta$, its influence on the wave process may be found rather substantial because it changes the exponential factor: $\exp\left[i\left(\widetilde{\beta}+\delta\beta\right)z\right]=\exp\left[i\left(\widetilde{\beta}+\delta\beta\right)z+2\pi\right]$.

From eq. (3.2) and (3.4) we obtain the polarization correction [67] in the form:

$$\begin{aligned}\delta\beta &= 2\Delta\int_S \widetilde{e}_i^{*}\partial_i f\partial_k\widetilde{e}_k dS \\ &= \int_S \left(e_x^{*}, e_y^{\bullet}\right)\begin{pmatrix}\partial_x f\partial_x & \partial_x f\partial_y \\ \partial_y f\partial_x & \partial_y f\partial_y\end{pmatrix}\begin{pmatrix}\widetilde{e}_x \\ \widetilde{e}_y\end{pmatrix}dS, \\ &= \left\langle\widetilde{\mathbf{e}}\middle|\hat{H}_{\text{int}}\middle|\widetilde{\mathbf{e}}\right\rangle\end{aligned} \quad (3.9)$$

where it was used $\nabla\ln n^2 = -2\Delta\nabla f$, $\widetilde{\mathbf{e}}\approx\mathbf{e}$ and the integration was carried over the whole space $0\le R<\infty$.

The operator $\hat{H}_{\text{int}}$ has a form:

$$\hat{\mathbf{H}}_{\text{int}} = \frac{1}{2}\frac{\partial f}{\partial r}\left(\hat{\boldsymbol{\sigma}}_0+\hat{\mathbf{T}}\right)\hat{\mathbf{D}}, \quad (3.10)$$

where $\hat{\mathbf{T}}=\begin{pmatrix}\cos 2\varphi & \sin 2\varphi \\ \sin 2\varphi & -\cos 2\varphi\end{pmatrix}_L$ in the linearly polarized basis (the subscript *L*), $\hat{\mathbf{T}}=\begin{pmatrix}0 & e^{-i2\varphi} \\ e^{i2\varphi} & 0\end{pmatrix}_C$ in the circular polarized basis (the subscript *C*) and $\hat{\mathbf{D}}=\hat{\boldsymbol{\sigma}}_0\frac{\partial}{\partial r}+\frac{i}{r}\hat{\boldsymbol{\sigma}}_3\frac{\partial}{\partial\varphi}$, $\hat{\boldsymbol{\sigma}}_0, \hat{\boldsymbol{\sigma}}_3$ - Pauli matrices.

Thus, the average value of the operator $\hat{\mathbf{H}}_{\text{int}}$ is equal to the polarization correction

The spin-orbit interaction in fibers not only lifts the degeneracy but it also changes the structure of the ground state itself. Indeed, the operator $\hat{\mathbf{D}}$ gives a contribution to the polarization correction $\delta\beta$ for the CV vortices (3.5) and any their superposition if $\kappa=+1$, while the effect of the operator $\hat{\mathbf{T}}$ on such states vanishes. On the other hand, the operator $\hat{\mathbf{T}}$ exerts a different influence upon the superposition of the nonuniform vortices $|+1,-1\rangle+|-1,+1\rangle$ and $|+1,-1\rangle-|-1,+1\rangle$ with the single topological charge $l=1$ generating the polarization corrections $\delta\beta_{TM}\neq 0$ and $\delta\beta_{TE}=0$, while the states $|+1,+1\rangle, |-1,-1\rangle$ are remain. The operator $\hat{\mathbf{D}}$ changes no $|+1,-1\rangle+|-1,+1\rangle$ and $|+1,-1\rangle-|-1,+1\rangle$ states. The eigenmodes found in these states are locally linearly polarized and are called the transverse magnetic *TM* and the transverse electric *TE* waves because either the *z*-component magnetic or *z*-component electric fields are zero. It should be noted that the degenerated $|+1,+1\rangle, |-1,-1\rangle$ vortices are realized with respect to parity. Since *TE* and *TM* modes have different propagation constants so that $\delta\beta_{TE}=0$ and β_{TM} - the curve 1, the nonuniform vortices in the steady states $|+1,-1\rangle, |-1,+1\rangle$ cannot exist. It means that the conversion of the topological charges and polarization states takes place as the nonuniform vortex propagates along the fiber [63].

Such a division of the guided vortices into two large groups is first of all caused by the spin – orbit interaction in the fiber that in turn has generic foundation in two energy whirls around both the fiber optical axis and the instantaneous normals to the helical wavefront representative of the topological charge l and helicity σ, respectively.

III.1.3 Topological Phase and Polarization Corrections

The complicated whirl movement in the guided vortex influences the phase velocity manifesting itself as additional phase deviations in the eigenmode field. In order to reveal this movement one writes the Poynting vector components of the guided vortex [72]:

$$\begin{aligned}P_r &= 0 \\ P_\varphi &= -\kappa\sigma K F_l(R)G_l^{(-\kappa)}(R), \\ P_z &= K\frac{V}{\sqrt{2\Delta}}F_l^2(R),\end{aligned} \quad (3.10a)$$

where $K=|E_0|^2\sqrt{\frac{\varepsilon_0}{\mu_0}}\frac{\sqrt{2\Delta}}{V}$, $G_l^{(-\kappa)}=\frac{dF_l}{dR}-\kappa\frac{l}{R}F_l$, E_0 - a mode amplitude. The current lines of the

Poynting vector depicted by Fig.8 emphasize the structure difference between the uniform and nonuniform vortex families. The fact is that the uniform vortex has the whole group of the spiral current lines rotating in the same direction while two groups of the spiral current lines of the nonuniform vortex are twisted towards each other. Moreover, the spiral pitch of the uniform vortex is the same for all lines while those of the nonuniform vortex may change from zero to infinity. Naturally, a such variety of rotatory movements cannot but have an effect on the motion of the vortex itself. The topological Berry's phase is the concentrated expression of any cyclic variations [18] including the whirl inside an optical vortex [67]. The topological nature of the Gouy phase in the paraxial Laguerre-Gaussian beams [48] takes on special sounding in the form of the *topological birefringence* [74] while the beam turns into the guided vortex. In this process the polarization corrections to the scalar propagation constant play the main role. Let us consider this problem more minutely.

From Fig.8 it can be seen that the Poynting vector performs a precessional motion around the fiber axis. Its behavior is similar to that of the wave vector of the fundamental HE_{11} mode in a coiled fiber [85,86]. The solid angle $\Omega(C)$ in momentum space C is spanned by the Poynting vector due to a spiral turn at the azimuth angle φ is [67]:

$$\Omega = \varphi\left(1-\frac{P_z}{P}\right), \quad P=\sqrt{P_z+P_\varphi}\,. \qquad (3.11)$$

If one denotes the specific topological phase (the phase per unit length of the trajectory in the momentum space) as $\theta = \partial\Omega/\partial z$ then the average value of θ is written in the form:

$$\langle\theta\rangle = \frac{\int\limits_\theta \theta\, P\, d\theta}{\int\limits_\theta P d\theta} = \langle\tilde{\mathbf{e}}_t|\hat{\mathbf{H}}_{\text{int}}|\tilde{\mathbf{e}}_t\rangle = \delta\beta\,. \qquad (3.12)$$

Thus, the specific topological phase of the guided vortices represents the polarization correction $\delta\beta$ to the scalar propagation constant $\tilde{\beta}$.

As for the nonuniform vortices with the single topological charge $l=1$, their total angular momentum $M_z = \langle \mathbf{r}\times\mathbf{P}/c^2\rangle_z$ consist of the sum of the orbital L_z and spin S_z angular momenta equal each other $L_z = -S_z$ and $M_z = L_z + S_z = 0$. Such a vortex with the zero angular momentum cannot stay in a steady state and breaks into *TE* and *TM* modes.

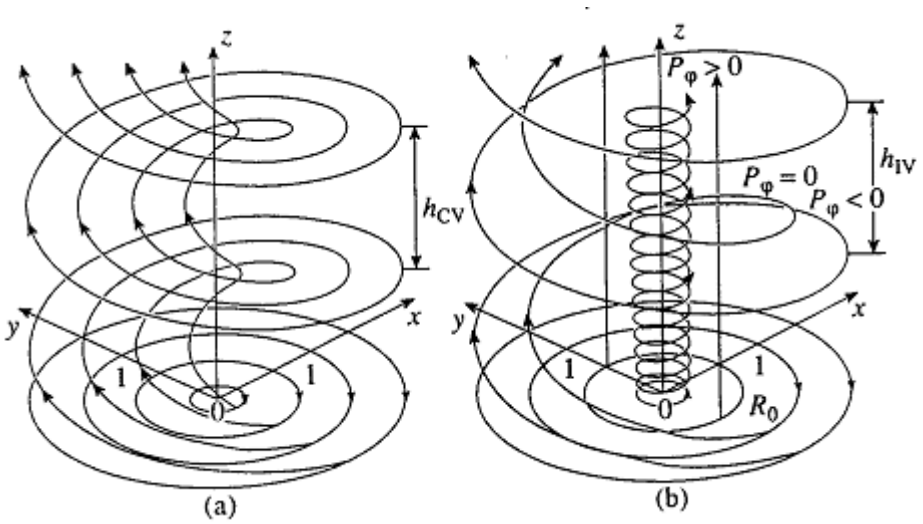

Fig.8. Current lines of the uniform (a) and nonuniform (b) guided vortex

III.2 Generic Guided Vortices in Perturbed Optical Fibers

Although optical vortices can be transmitted through the ideal circular locally isotropic fiber at arbitrary long distances, any slight perturbations of the fiber may cause vortex decay. Therefore, it is better to speak about the *lifetime* or *lifelength* of a *generic vortex* [2] that can slowly or quickly change its structure as it propagates along a real fiber. For instance, an external mechanical influence upon the fiber can produce its deformation, cabling, bending and other imperfections, provoking in that way, variations of a refractive index profile and a cross-section form. Naturally such perturbations change the spectrum structure of both eigenmodes and eigenvalues. It is very difficult, without some analytical calculations, to predict what will be the spectrum form in a perturbed fiber. The most vivid example of erroneous prediction in fiber singular optics is utilization of analogies. Thus, it is well known that any geometrical [87], stress-induced [88,89], thermally induced [90,91], bent-induced [92-95], twisted-induced [96-98] and other perturbations take away the degeneracy over polarization from a single mode fiber and force a polarization-mode dispersion. However, strong uniform tensions inside a fiber core [99] suppress an energy conversion from one orthogonal linear polarization to another preserving a linearly polarized HE_{11} mode. It would be quite reasonable by analogy with the single mode fiber to suppose that a stress-induced low-mode fiber will maintain also a linearly polarized optical vortex. Nevertheless, as it has been shown in the work [78] such an assumption cannot be right and a physical mechanism prohibitive to do so, is the spin – orbit interaction.

To see this one should consider in some detail the mechanism of the level-reconstruction of the propagation constant β and transformations of the wave vectors $|\Psi_l\rangle$ in an optical fiber subjected to some deformations of its cross-section geometry [78], a core-clad-anisotropy [100] and bend [79] perturbations. As a matter of fact, some variations of the fiber geometry are somehow or other reflected on anisotropic properties of the fiber material at the expense of the photoelastic effect. Because of it the geometry deformations, the bend and the fiber cabling cause stress-induced anisotropy. Nevertheless, in many cases it is possible to study these processes separately.

III.2.1 Fiber Material Anisotropy

The aim of this section is to discuss some fine physical mechanisms of generic vortex behavior in a weakly guiding fiber.

Consider a fiber with a weak anisotropy so that its permittivity is $\hat{\varepsilon} = \widetilde{\varepsilon} \cdot \hat{1} + \delta\hat{\varepsilon}$ and $\widetilde{\varepsilon} >> \delta\varepsilon_{ik}$. One also considers that the anisotropy axes are directed along the coordinate axes where the tensor $\hat{\varepsilon}$ is the diagonal one: $\hat{\varepsilon} = \mathrm{diag}(\varepsilon_e, \varepsilon_o, \varepsilon_o)$. The wave equation (3.2) is written in the form:

$$\left((\nabla^2 + \nu^2(x,y)k^2\hat{\mathbf{1}}) + \delta\nu^2\hat{\boldsymbol{\sigma}}_z + \hat{\mathbf{U}}\right)|\mathbf{e}_t\rangle = \beta^2|\mathbf{e}_t\rangle, \quad (3.13)$$

where $\nu^2(x,y) = (n_e^2 + n_o^2)(1 - 2\Delta f(x,y))/2$, $\delta\nu^2 = (n_e^2 - n_o^2)/2$, $\hat{\boldsymbol{\sigma}}_z$ is Pauli matrix, $\hat{\mathbf{U}} = \begin{pmatrix} \nabla_x \cdot g_x & \nabla_x \cdot g_y \\ \nabla_y \cdot g_x & \nabla_y \cdot g_y \end{pmatrix}$, $g_\alpha \equiv \dfrac{\partial \ln n^2}{\partial \alpha}$, $|\mathbf{e}_t\rangle = \begin{pmatrix} e_x \\ e_y \end{pmatrix}$. The weakly guiding fiber approximation: $n_{co} \approx n_{e,o}$ and $n_{co}^2 + n_{cl}^2 \approx 2n_{co}^2$ [82] enables us to rewrite eq. (3.13) as

$$\left(\hat{\mathbf{H}}_0 + \delta\nu^2\hat{\boldsymbol{\sigma}}_x + \hat{\mathbf{V}}\right)|\Psi\rangle = \beta^2|\Psi\rangle, \quad (3.14)$$

where $\hat{\mathbf{H}}_0 = (\nabla^2 + k^2 n^2(x,y)\hat{\mathbf{1}})$, $\hat{\mathbf{V}} = \mathbf{C}\hat{\mathbf{U}}\mathbf{C}^+$, $\mathbf{C} = \dfrac{1}{\sqrt{2}}\begin{pmatrix} 1 & -i \\ 1 & i \end{pmatrix}$ and the eigenvectors are written in the circularly polarized basis. The equation (3.14) is the equation for the

eigenvalues β^2 of the operator $\hat{\mathbf{H}} = \hat{\mathbf{H}}_0 + \hat{\mathbf{H}}_{\text{int}}$. While the levels β^2 are degenerated in view of lacking perturbations, "switching on" the perturbations takes away the degeneracy splitting the levels. It is convenient to choose the following guided vortices of the non-perturbed fiber as the basis of the generic vortex for the given topological charge l:

$$\begin{aligned}&|\Psi_1\rangle \equiv |+1,+l\rangle, |\Psi_2\rangle \equiv |+1,-l\rangle, |\Psi_3\rangle \\ &\equiv |-1,-l\rangle, |\Psi_4\rangle \equiv |-1,+l\rangle\end{aligned} \qquad (3.15)$$

and set the normalization requirement in the form: $2\pi \int_0^\infty RF_l^2(R)dR = 1$.

Now the perturbed part of the operator is

$$\begin{aligned}\hat{\mathbf{H}}_{\text{int}} &= -(\Delta\psi + (\Delta/2)r^2\chi)\hat{\mathbf{1}} + \\ &+ k^2 n_{co}(n_e - n_o)\hat{\boldsymbol{\sigma}}_x - \Delta\psi \hat{l}_z \hat{\boldsymbol{\sigma}}_z \\ &-(\Delta/2)r^2\chi\begin{pmatrix} 0 & e^{-2i\varphi} \\ e^{2i\varphi} & 0 \end{pmatrix},\end{aligned} \qquad (3.16)$$

where $\chi \equiv \frac{1}{r}\frac{\partial\psi}{\partial r}$, $\psi \equiv \frac{1}{r}\frac{\partial f}{\partial r}$, $\hat{l}_z = -i\frac{\partial}{\partial\varphi}$ is the z-component of the orbital angular momentum operator.

The matrix of the operator $\hat{\mathbf{H}}_{\text{int}}$ has the following structure:

$$\delta\hat{\mathbf{H}} = \begin{pmatrix} A_l & 0 & 0 & E_l \\ 0 & B_l & E_l & G_l \\ 0 & E_l & A_l & 0 \\ E_l & G_l & 0 & B_l \end{pmatrix}, \quad l = 1;$$

$$\delta\hat{\mathbf{H}} = \begin{pmatrix} A_0 & E_0 \\ E_0 & B_0 \end{pmatrix}, \quad l = 0. \qquad (3.17)$$

The corrections $\delta\beta^2$ to the scalar part $\tilde{\beta}^2$ are defined by the transcendental equation:

$$\det|(\hat{\mathbf{H}}_{\text{int}})_{ij} - \delta_{ij}\beta^2| = 0. \qquad (3.18)$$

Tables 1 and 2 illustrate the eigenvectors $\langle\Psi_l|$ and eigenvalues β_l^2 of the anisotropic fiber operator. The behavior of the eigenmodes is characterized by the dispersive curves $\beta(V)$ represented on the Fig.9 showing that even a very small birefringence $\delta n = n_e - n_o \propto 10^{-8}$ forces to split the level of CV vortex into even and odd parts shifting the *TM* mode level a little. The TE mode level responds to the perturbation only for a comparatively large birefringence $\delta n \propto 10^{-6} \div 10^{-4}$.

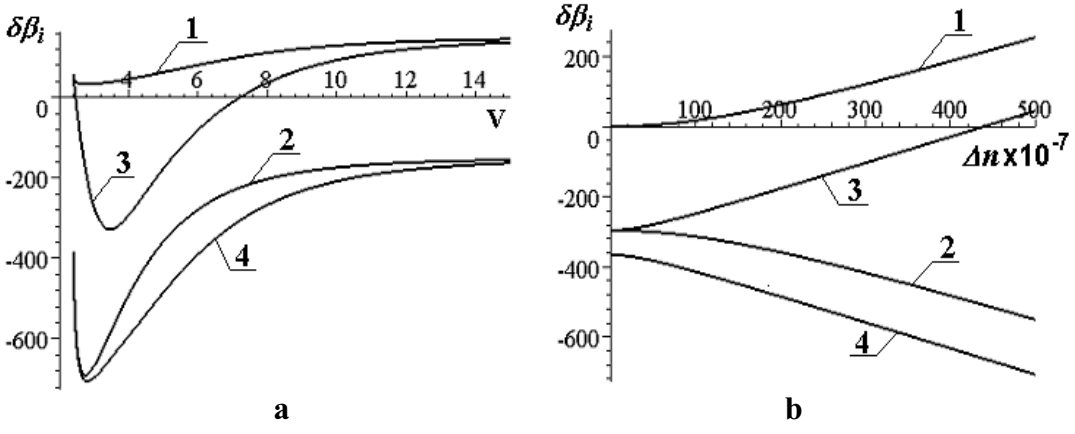

Fig.9. Dispersive curves for the anisotropic fiber as (a) the dependency of the polarization correction $\delta\beta\ (m^{-1})$ on the waveguided parameter *V* (in non-dimensional units) and $\delta n = 2\cdot 10^{-5}$; (b) the dependency $\delta\beta$ on the birefringence δn (*V=5,* $\Delta = 0.01$).The curve 1 corresponds to the state $|1\rangle$, curve 2 – $|3\rangle$, curve 3 – $|2\rangle$, curve 4 – $|4\rangle$.

Table 1. Eigenmode fields of anisotropic, elliptic and bent fibers

	$\frac{1}{\sqrt{2}F_l(R)}\,\tilde{\mathbf{e}}_t$	$\frac{2}{\sqrt{2}}\frac{k\rho}{i}\,e_z$	$\frac{1}{\sqrt{2}\,F_l(R)}\frac{1}{n_{co}}\sqrt{\frac{\mu_0}{\varepsilon_0}}\,\tilde{\mathbf{h}}_t$	$\frac{2}{\sqrt{2}}\frac{ik\rho}{n_{co}}\sqrt{\frac{\mu_0}{\varepsilon_0}}\,h_z$	$\Delta\beta_i^2=\beta^2-\tilde{\beta}^2$
1	$\mathbf{n}_x\cos\vartheta\sin l\varphi$ $+\mathbf{n}_y\sin\vartheta\cos l\varphi$	$\Im^+\sin(l+1)\varphi\,G_l^-$ $+\Im^-\sin(l-1)\varphi\,G_l^+$	$\mathbf{n}_x\sin\vartheta\cos l\varphi$ $-\mathbf{n}_y\cos\vartheta\sin l\varphi$	$\Im^+\cos(l+1)\varphi\,G_l^-$ $-\Im^-\cos(l-1)\varphi\,G_l^+$	$\frac{1}{2}\Theta_{1l}+\frac{1}{2}\Xi_{1l}$
2	$-\mathbf{n}_x\sin\vartheta\sin l\varphi$ $+\mathbf{n}_y\cos\vartheta\cos l\varphi$	$-\Im^-\sin(l+1)\varphi\,G_l^-$ $+\Im^+\sin(l-1)\varphi\,G_l^+$	$\mathbf{n}_x\cos\vartheta\cos l\varphi$ $+\mathbf{n}_y\sin\vartheta\sin l\varphi$	$\Im^-\cos(l+1)\varphi\,G_l^-$ $+\Im^+\cos(l-1)\varphi\,G_l^+$	$\frac{1}{2}\Theta_{1l}-\frac{1}{2}\Xi_{1l}$
3	$\mathbf{n}_x\cos\vartheta\cos l\varphi$ $-\mathbf{n}_y\sin\vartheta\sin l\varphi$	$\Im^+\cos(l+1)\varphi\,G_l^-$ $+\Im^-\cos(l-1)\varphi\,G_l^+$	$\mathbf{n}_x\sin\vartheta\sin l\varphi$ $+\mathbf{n}_y\cos\vartheta\cos l\varphi$	$\Im^+\sin(l+1)\varphi\,G_l^-$ $-\Im^-\sin(l-1)\varphi\,G_l^+$	$\frac{1}{2}\Theta_{2l}+\frac{1}{2}\Xi_{2l}$
4	$\mathbf{n}_x\sin\vartheta\cos l\varphi$ $+\mathbf{n}_y\cos\vartheta\sin l\varphi$	$-\Im^-\cos(l+1)\varphi\,G_l^-$ $+\Im^+\cos(l-1)\varphi\,G_l^+$	$\mathbf{n}_x\cos\vartheta\sin l\varphi$ $-\mathbf{n}_y\sin\vartheta\cos l\varphi$	$\Im^-\sin(l+1)\varphi\,G_l^-$ $+\Im^+\sin(l-1)\varphi\,G_l^+$	$\frac{1}{2}\Theta_{2l}-\frac{1}{2}\Xi_{2l}$

$\Theta_{li}=A_l+(1-\gamma_i)B_l\,;\Xi_{li}=\sqrt{\left[-A_l+(1-\gamma_i)B_l\right]^2+4E_l^2}$, $Q_l\equiv E_l$ - *anisotropic fiber;* $\gamma_i=\begin{cases}+1, i=1,2\\-1, i=3,4\end{cases}$,

$\Theta_l=A_l+B_l-\gamma G_l\quad \Xi_l=\sqrt{\left(-A_l+B_l-\gamma G_l\right)^2+4\left(D_l-\gamma E_l\right)^2}$, $Q_l\equiv E_l-\gamma D_l$ - *elliptic and bent fiber.*

$\Im^{\pm}=\cos\vartheta\pm\sin\vartheta\,;\tan 2\vartheta=X$, $X=\dfrac{A_l+B_l-\gamma G_l}{2Q_l}$, $2\vartheta\in\left[0,\pi\,\mathrm{sign}\,Q_l\right]$, $G_l^{\pm}=\dfrac{dF_l}{dR}\pm\dfrac{l}{R}F_l$, $F_l(R)=\dfrac{J_l(\tilde{U}R)}{j_l(\tilde{U})}$,

$$R=\frac{r}{\rho}.$$

It is not unreasonable to consider two utmost cases of the weak and strong fiber anisotropy. The *weak anisotropy* corresponds to the requirement: $\delta n<<\Delta(\lambda/\rho)^2$ while the *strong anisotropy* is - $\Delta(\lambda/\rho)^2<<\delta n<<1$, ρ - fiber radius. The weak anisotropy in fact leaves alone a permanent structure of the eigenmodes of a non-perturbed fiber varying only in the polarization correction values. The strong anisotropy, besides, transforms the eigenmode structure unless the modes become linearly polarized fields:

$$|\Psi_1\rangle\propto\begin{pmatrix}\sin\varphi\\0\end{pmatrix},\qquad |\Psi_2\rangle\propto\begin{pmatrix}0\\\cos\varphi\end{pmatrix},$$

$$|\Psi_3\rangle\propto\begin{pmatrix}\cos\varphi\\0\end{pmatrix},\qquad |\Psi_4\rangle\propto\begin{pmatrix}0\\\sin\varphi\end{pmatrix}.$$

The main distinguishing feature of the vortex is its angular momentum $\mathbf{M}=\mathbf{r}\times\mathbf{P}/c^2$ that can be divided into orbital and spin parts (for the weakly guiding fiber) so that $M_z=L_z+S_z$. The orbital angular momentum is defined as (l=1)

$$\begin{aligned}L_z&=\left\langle\hat{L}_z\right\rangle=\langle\Psi|\hat{L}_z|\Psi\rangle=i\langle\Psi|\frac{\partial}{\partial\varphi}|\Psi\rangle=\\&=\cos\left(\vartheta-\tilde{\vartheta}\right)\begin{Bmatrix}\cos\vartheta\cos\tilde{\vartheta}\cos\beta_{13}z\\+\sin\vartheta\sin\tilde{\vartheta}\cos\beta_{24}z\end{Bmatrix}+\\&+\sin\left(\vartheta-\tilde{\vartheta}\right)\begin{Bmatrix}\sin\vartheta\cos\tilde{\vartheta}\cos\beta_{23}z\\+\cos\vartheta\sin\tilde{\vartheta}\cos\beta_{14}z\end{Bmatrix}\end{aligned}\qquad(3.19)$$

for the *x*- or *y*- polarized optical vortex. The spin angular momentum of such a vortex can be found as

$$\begin{aligned}\left\langle S_z\right\rangle&=\langle\Psi|\hat{\boldsymbol{\sigma}}_z|\Psi\rangle\\&=\sin(\theta+\tilde{\theta})\left[\cos\theta\cos\tilde{\theta}\cos\delta\beta_{13}z\right.\\&\left.-\sin\theta\sin\tilde{\theta}\cos\delta\beta_{24}z\right]-\\&-\cos(\theta+\tilde{\theta})\left[\cos\theta\sin\tilde{\theta}\cos\delta\beta_{14}z\right.\\&\left.+\sin\theta\cos\tilde{\theta}\cos\delta\beta_{23}z\right]\end{aligned},\qquad(3.20)$$

where we denote $\delta\beta_{ij}=\delta\beta_i-\delta\beta_j$, the value ϑ

Table 2. Matrix elements of the spin – orbit operator $\delta\hat{\mathbf{H}}$ for a perturbed fiber

<table>
<tr><td colspan="2">$A_l = -\frac{\Delta}{r_0^{\,2}}\left(F_l^{\,2} - F_l F_l^{'}\right)_{R=1}$ $\qquad$ $B_l = \frac{\Delta}{r_0^{\,2}}\left(F_l^{\,2} + F_l F_l^{'}\right)_{R=1}$</td></tr>
<tr><td>Elliptic fiber $l = 1,2$</td><td>Anisotropic fiber $l = 1$</td></tr>
<tr><td>$C_l = 0$;
$D_l = \pi k^2 n_{co}^{\,2}\delta^2\Delta\left(a_l F_l^{\,2} + b_l F_l F_l^{'}\right)_{R=1}$;
$E_l = -\frac{\pi\delta\Delta}{r_0^{\,2}}\left(F_l F_l^{''} + F_l^{'2} - F_l F_l^{'}\right)_{R=1}$
$G_l = \frac{2\pi\delta\Delta}{r_0^{\,2}}\left\{p_l F_l^{\,2} + d_l F_l F_l^{'} - 2b_l\left(F_l^{'2} + F_l F_l^{''}\right)\right\}_{R=1}$</td><td>$E_1 = n_o k^2\Delta n$, $C_1 = D_1 = 0$
Bent fiber l=1
$D_l = 4k^2 n_{co}^{\,2}\left(1+\mu^{-1}\right)\left(\frac{r_0}{R_0}\right)^2\int_0^\infty R^3 F_1^2(R)\,dR$
$G_l = \frac{\Delta}{r_0^{\,2}}\left\{F_l^{\,2} + F_l F_l^{'}\right\}_{R=1}$, $C_1 = E_1 = 0$,
R_0 - radius of a bend</td></tr>
<tr><td colspan="2">$a_l = \begin{cases} -\frac{2}{\delta}, l=1 \\ \frac{5}{2}, l=2 \end{cases}$; $b_l = \begin{cases} 0, l=1 \\ 1, l=2 \end{cases}$; $d_l = \begin{cases} \frac{1}{\delta}, l=1 \\ -14, l=2 \end{cases}$; $\quad p_l = \begin{cases} \frac{1}{\delta}, l=1 \\ -8, l=2 \end{cases}$, $\Delta n = n_e - n_o$</td></tr>
</table>

corresponds to *i=1,2*, while $\tilde{\vartheta}$ - to *i=3,4* (see Table 1). The angular momenta are given as normalized quantities in eqs. (3.19) and (3.20). The orbital angular momentum in the fiber with the weakly anisotropy changes to $L_z \approx \cos^2\left(B_1/2k\right)z$ and the spin momentum – to $S_z = \sin^2\frac{B_1}{2k}z$. Since the value B_1 does not depend on the anisotropy δn the angular momentum varies in the same way as it changes in the ideal fiber [72]. The strong anisotropy offers an other plot of the vortex evolution. So, the orbital momentum has oscillations in the form $L_z \approx \cos\left(B_1/2k\right)z$ while the spin momentum is entirely suppressed. This process can be traced in detail by the course of the discriminatory curves depicted in Fig.10. Thus, the oscillating nature of the angular momentum shows that the anisotropic fiber cannot preserve a linearly polarized guided vortex.

III. 2.2. Geometrical Birefringence

The influence of geometry upon the optical anisotropy of different objects has been more than once stressed in a lot of experiments (see, for example, the work [3]) and was called the birefringence of the form. Only recently its systematic study begins due to single mode fibers. The fact is that some geometry variations of a fiber cross-section stimulate the polarization-induced dispersion and thereby restrict the information transmission rate within a narrow range. They also play an important role in limiting the vortex lengthlife. Although the geometric influence manifest itself simultaneously with the anisotropic one it is sometimes useful to consider its separately [78,100].

Provided that a perturbation of cross-section geometry is very small then we can choose the refractive index profile of a fiber in the form:

$$f(x,y) \Rightarrow f\left(x(1+\delta), y(1-\delta)\right) \qquad \text{and} \quad \delta << 1$$

$$\approx \tilde{f}(\mathbf{r}) + \left(\frac{\partial\tilde{f}}{\partial x}x - \frac{\partial\tilde{f}}{\partial y}y\right)\delta,$$

while the function $\tilde{f}$ describes a non-perturbed profile. The ellipse eccentricity e and the parameter δ are connected with each other by $\delta \approx e^2/4$. Then the operator of the spin – orbit interaction can be written as

$$\hat{\mathbf{H}}_{\text{int}} = \begin{matrix} -\Delta\psi\,\hat{l}_z\hat{\boldsymbol{\sigma}}_z - (\Delta/2)r^2\chi\begin{pmatrix} 0 & e^{-2i\varphi} \\ e^{2i\varphi} & 0 \end{pmatrix} - \Delta\delta\left\{\begin{matrix}\left[2{n_{co}}^2 r^2\psi k^2 + \dfrac{\left(r^6\chi\right)'}{2r^3}\right]\cos 2\varphi\cdot\hat{\mathbf{1}} \\ +\left(2\widetilde{f}'' + \dfrac{1}{4}r^3\chi'\right)\hat{\boldsymbol{\sigma}}_x + \dfrac{1}{4}r^3\chi'\begin{pmatrix} 0 & e^{-4i\varphi} \\ e^{4i\varphi} & 0 \end{pmatrix}\end{matrix}\right\}. \\ -\left[\Delta\psi + (\Delta/2)r^2\chi\right]\hat{\mathbf{1}} \end{matrix} \quad (3.21)$$

The matrix of this operator has a form

$$\delta\widehat{\mathbf{H}} = \begin{pmatrix} A_l & D_l & C_l & E_l \\ D_l & B_l & E_l & C_l + G_l \\ C_l & E_l & A_l & D_l \\ E_l & C_l + G_l & D_l & B_l \end{pmatrix}. \quad (3.22)$$

The eigenvectors are defined as the superposition of the eigenvortices of a non-perturbed fiber and the polarization corrections – by eq.(3.18) that are presented by Table 1 and 2.

As it has been in the case with the material anisotropy two limiting situations can be singled out: the *weak ellipticity*: $\delta << (\lambda/\rho)^2$ and the *strong ellipticity* $(\lambda/\rho)^2 << \delta << 1$. In connection with this, it would be interesting to discuss the problem of the angular momentum of the circularly polarized generic vortex.

The generic vortex state using Tables 1 and 2 can be written in the case of the weak ellipticity as

$$\begin{matrix}|1,l\rangle^{ell} = \{\ |1,l\rangle\cos\delta\beta_{24}z + \\ +\,i|-1,-l\rangle\sin\delta\beta_{24}z\ \}\exp\{i(\widetilde{\beta}+\beta_{24})z\}\end{matrix} \quad (3.23)$$

so that the total angular momentum is $M_z{}^{ell} \approx \cos\delta\beta_{24}z$ while the spin and orbital momenta have a form: $S_z \approx \cos\delta\beta_{13}z$ and $L_z \approx -\cos\delta\beta_{13}z$, respectively.

The strong ellipticity case gives the generic vortex state in the form:

$$\begin{matrix}|1,l\rangle^{ell} = \frac{1}{4}\{|1,l\rangle\left(e^{i\beta_1 z} + e^{i\beta_2 z} + e^{i\beta_3 z} + e^{i\beta_4 z}\right) + \\ |-1,-l\rangle\left(-e^{i\beta_1 z} - e^{i\beta_2 z} + e^{i\beta_3 z} + e^{i\beta_4 z}\right) + \\ |1,-l\rangle\left(e^{i\beta_1 z} - e^{i\beta_2 z} + e^{i\beta_3 z} - e^{i\beta_4 z}\right) + \\ |-1,l\rangle\left(-e^{i\beta_1 z} + e^{i\beta_2 z} + e^{i\beta_3 z} - e^{i\beta_4 z}\right)\ \}\end{matrix} \quad (3.24)$$

and the spin and orbital momenta become $S_z \approx \cos(B_1/2k)z$ and $L_z \approx \cos(D_1/k)z\,\cos(B_1/2k)z$, respectively, so that the total angular momentum is $M_z \approx 2\cos^2(D_1/2k)z\cos(B_1/2k)z$.

The results obtained enable us to conclude that the circular polarized fiber vortices cannot also propagate without any structure variations along the geometrically perturbed fiber. The oscillations of the orbital and spin angular momenta point out the energy conversion both between a positive and negative value of the topological charge and the right and left polarization states. There exists a wave state with zero angular momentum when the vortex as such has disappeared. Fig.11 schematically illustrates the conversion process of the orbital angular momentum L_z of the generic vortex that manifests itself by variations of the intensity distribution at the cross-sections of the fiber straight region. So, the generic vortices with opposite topological charges in series are swapped around passing through the wave state with a pure edge dislocation. However the topological charge and helicity are inseparably linked with each other in the optical fiber [27]. Consequently, state polarization also experiences a helicity transformation [26]. It means that the spin angular momentum takes part in this conversion process too. At the same time, the orbital and the spin momenta have different oscillation frequencies both having an irrational ratio in general case. Because of it the initial vortex state cannot be recovered at any fiber cross-sections though it may approach rather close to the initial one. Besides, the state with a pure edge dislocation bears no orbital angular momentum, but this does not necessarily mean that the spin momentum is zero. Just the opposite, the spin momentum at this cross-sec-

tion may be the highest possible. Moreover, the total angular momentum is not conserved both in an elliptic and an anisotropic fiber as a rule.

III.2.3. Bent Optical Fibers

The optical fiber used in real fiber-optical devices as a rule undergoes a mechanical bend and cabling that cause a stress-induced birefringence and, consequently, levels of the propagation constant must experience a splitting and a shift. The bent fiber problem discussed in detail for single-mode fibers (some of the works are [92-95]) has been considered for fiber vortices only in the works [79,102,103]. Nevertheless we shall endeavour to make this topic clear. The twisted fiber problem will be discussed briefly in the next section. Thus we shall neglect a stress-induced anisotropy.

We should focus our attention on three main physical mechanisms manifesting themselves due to the fiber bend: a curved geometry of the bent fiber, an asymmetry of the refractive index profile and a stress-induced anisotropy. In one form or another the influence of these factors upon the birefringent have been already taken into account in the numerous works on a single mode fiber (see, for example, the works [92-95] and the references to them). The influence of geometry upon the mode field lies in a different respond of light field components on the curved-fiber space – the component lying in the plane of the bend and orthogonal to it have different phase and group velocities. In other words, an optical path increases for one of the field components. The asymmetry of a refractive index profile originates from differences of an optical density of a fiber cross-section near the bend center and at some distance from it.

The model of a bent fiber [79] accounts for the fact that practically in most often met situations the bending does not destroy the transport properties of the fiber and is manifested as a perturbation on the background of a stable state. It has to be based also on the assumption of translatory invariance along the fiber axis.

The refractive index of a bent fiber can be transformed into the refractive index of a straight fiber in the wave equation (3.2) in the following way:

$$n(x,y)=\left(1+\frac{x}{\rho}\right)^{-1}\left(1+\frac{x}{\rho}(1-2\mu)\right), \qquad (3.25)$$
$$\tilde{n}\left(x-u_x, y-u_y\right)$$

where $u_{zz}=x/\rho$, $u_{xx}=u_{yy}=-\mu u_{zz}$, μ is the Poisson coefficient. Asearlier the basis vectors are chosen in the form of guided vortices of a

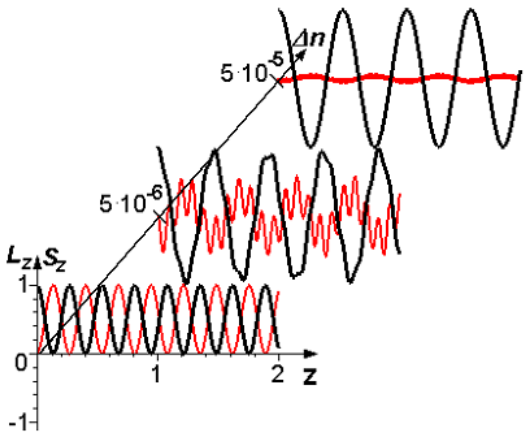

Fig.10. The orbital L_z (the curve 1) and spin S_z (the curve 2) angular momentum evolution (in relative units) of the linear polarized vortex as the function of the fiber length *z* (m) and the anisotropy δn

non-perturbed fiber. Then the spin – orbit operator gains the form:

$$\begin{aligned}\hat{\mathbf{H}}_{\text{int}} &= k^2\left(n^2-\tilde{n}^2\right)\hat{\mathbf{1}}+\\ &+\frac{1}{4}\left\{\left[\left(\ln n^2\right)_{xx}+\left(\ln n^2\right)_{yy}\right]\hat{\mathbf{1}}+\right.\\ &+\left[\left(\ln n^2\right)_{xx}-\left(\ln n^2\right)_{yy}\right]\hat{\boldsymbol{\sigma}}_x \qquad (3.26)\\ &+2\left(\ln n^2\right)_{xy}\hat{\boldsymbol{\sigma}}_y+\\ &\left.+2i\left[\left(\ln n^2\right)_y\nabla_x-\left(\ln n^2\right)_x\nabla_y\right]\hat{\boldsymbol{\sigma}}_z\right\}\end{aligned}$$

where $f_u \equiv \dfrac{\partial f}{\partial u}$. The eigenmodes, the polarization corrections and the matrix elements of the operator (3.26)

$$\delta\hat{\mathbf{H}}=\begin{pmatrix} A_l & D_l & C_l & E_l \\ D_l & B_l & E_l & C_l+G_l \\ C_l & E_l & A_l & D_l \\ E_l & C_l+G_l & D_l & B_l \end{pmatrix} \qquad (3.27)$$

are introduced in Tables 1 and 2.

The behavior of the curves is similar to those both in an anisotropic and an elliptic fiber, at any rate the bend takes the degeneracy off the propagation constant level making it oscillate the spin and orbital angular momenta. Naturally, the optical vortices in these fibers are not eigenmodes and break up into eigen modes of the perturbed fiber that have the same mathematical form for all the above considered perturbations.

IV. Forecasts and Prospects

The unique properties of optical vortices open a variety of new possibilities for their application. For example, the form of the laser beam bearing an optical vortex is similar to one of a potential hole for trapped cold atoms. Several constructions of such optical traps have been more than once proposed and experimentally realized (see the work [22] and the reference to it). Moreover, optical vortices became the physical instrument to create optical tweezers and spanners able to trap, transport and twist microscopic particles having sizes up to $50\,\mu m$ (see the works [20,22,23,106] and references to them). Application of optical fibers in such constructions could greatly enlarge the functional scope of these devices. However, guided fiber vortices themselves possess utterly unique properties distinguishing them from vortices in free space [81, 107-110] that can be called for different fiber-optical devices as *optical gyroscopes* and other sensors of physical values.

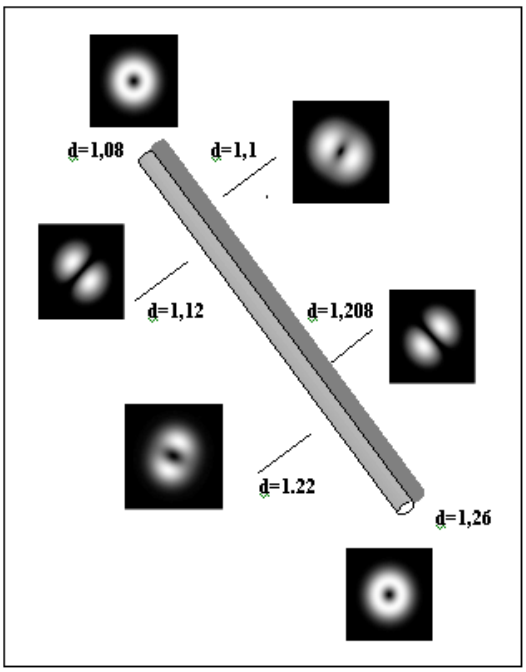

Fig.11. The conversion of the orbital angular momentum L_z of the generic vortex in the state $|+1,+1\rangle$ along the beat length Λ (in meters) for the strong ellipticity case: $\Delta = 0.01$; $n_{co} = 1.48$, $e = 0.1$.

IV.1. Fiber-Vortex Temperature Sensor

Consider briefly the fiber-vortex temperature sensor [107-111] on the example of which we make the acquaintance of the main peculiarities of this sort of device.

Fig.12 depicts the optical scheme of this interferometric sensor. We can distinguish four major optical units: 1) the optical vortex generation unit, 2) the excitation and light guiding unit, 3) the vortex selection unit and 4) the data processing unit. The first and second units we have discussed in Sec.II.5 and III, respectively. The last unit has its specific traits and it is a computer engineering area rather than optics

[109,110]. Let us focus our attention on the optical vortex selection unit placed on a fiber output.

The fact is that the slight displacement of the excitation beam on a fiber input relative to its axis causes the appearance of additional noise generic vortices in the fiber canal even if any strong mechanical perturbations are absent. Thus, both constrained and free vortices are propagated in the fiber. The constrained vortices combine symmetric topological dipoles and quadruples [20, 22, 81, 111] while the joining of the free vortex to these topological pairs distorts them and the asymmetric dipole or quadruple is formed. The typical vortex trajectories in a symmetric topological dipole are shown on Fig.13a. As a rule, there exist forbidden and confident zones in such topological structures. At the edges of these zones the optical vortex pairs are born or die. In the given case the vortices intersect the focal plane in the points lying symmetrically relative to the optical axis. These vortices have opposite topological charges, their interference spirals are wound round in opposite directions and hinder interference measurements. Quite another pattern of the propagation process of an asymmetric quadruple is depicted in Fig.13b. Like in the first case there exist the confident and forbidden zones but energy is redistributed in another way among the optical vortices. The larger energy portion has an associated free vortex. As fast as the topological pairs come near the focal plane the associated free vortex snuggles up to the axis while the rest of the vortices are forced out to the periphery, losing energy. The interference pattern becomes, essentially clearer and accuracy of the interference measurement increases greatly. In practice [108] two short-focussing lenses placed at the fiber output accomplish this mode selection. However, in contrast to an ordinary vortex filtration [61] this approach demonstrates the vortex self-recovery because no all the energy disappears but is only redistributed.

A temperature interferometric measurement of a low-mode fiber maintaining about eight modes including the work guided vortex was made in the work [108] and the result obtained showed that the temperature sensibility is almost twice as much as the typical single-mode sensor [90, 91]. In spite of such high experimental estimations, the practical applications of the fiber-vortex sensors are more than modest because these devices are unstable to some mechanical vibrations and other accidental hindrances. One must try to elucidate the cause of such vortex-sensor behavior. Among the causes most likely to be at fault is the explotable optical fiber itself. It is only the ideal circular fiber and its perturbed variants, that cannot maintain a single optical vortex!

IV.2. Vortex Preserving Fibers

In order to preserve a single guided vortex in a low-mode fiber it is necessary to suppress the rest of the eigenmodes and in the first place *TE* and *TM* fields. As a matter of fact these modes are simultaneously excited by the guided vortex in the fiber and cause a major noise. Besides, a fundamental HE_{11} mode (having no cut-off and being constantly in a fiber) displaces a vortex center and takes away a portion of the energy from it. However, the energy distributions of the *TE* and *TM* modes differ from those in the vortex. Though transverse components of the wave functions both in the vortex and in these modes have zero value at the fiber axis, the longitudinal components in the transverse modes are maximal. Moreover, a transverse component of the HE_{11} mode is maximal there too. The authors of the work [112] have proposed a way to cause energy losses of the noise modes at the expense of an impurity absorption in the vicinity of a fiber axis. This is easily accomplished by causing an impurity absorption in a waveguide core while manufacturing a fiber. In this fiber the noise modes are extinguished thousands of times faster than the guided vortex.

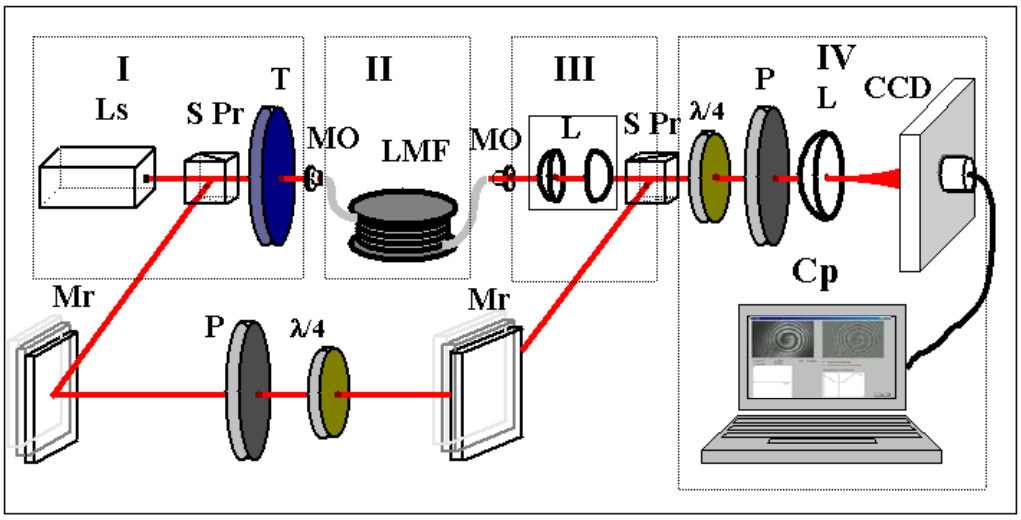

Fig.12. Sketch of the fiber – vortex temperature interferometer: Ls – He-Ne laser, S Pr – beam's splitter, T – vortex transparent, MO - $20^{\times}$ microobjective, Mr – mirror, CCD – camera, L – lens, $\lambda/4$ - $\lambda/4$ plate, Cp – computer. (I – the vortex generation unit, II – the vortex excitation and guiding unit, III- the vortex selection unit, IV – the computer-data processing unit)

At the same time, there are other possibilities to preserve a single guided vortex in a fiber. Thus, a single-mode fiber has been shown [113-115] to enable us to maintain an only circularly polarized mode provided that a core of an elliptical fiber is twisted around its optical axis with a certain pitch. The cabling of a low-mode fiber is connected with a number of surprises that can be after all overcome [80, 81] and special spun-fiber types may be exploited in fiber sensors as supersensitive elements as for example, in the work [116]. The three types of fiber core preserving a single vortex are illustrated in Fig.14. It is relatively simple to give an estimation of the requirements for a vortex preserving fiber. Consider it on the example of a core-spiral fiber [81].

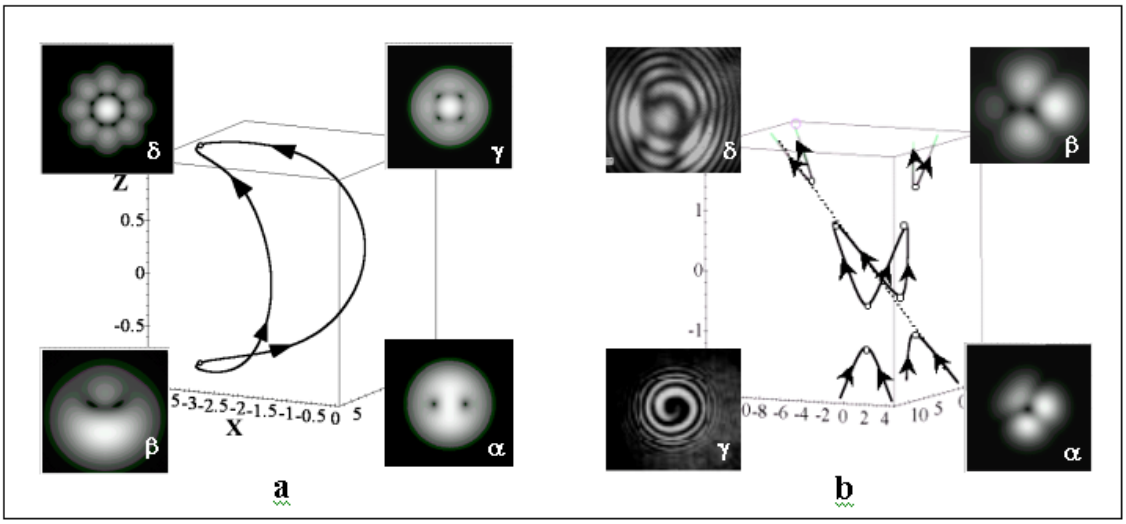

Fig.13. Vortex trajectories: (a) the symmetric topological dipole (at the center); its intensity distributions at the focus plane $z=0$ (α) and in the vicinity of the birth point $z=z_0$ (β); the topological quadruple (γ) and octople (δ) ; (b) the asymmetric topological quadruple (at the center); its theoretical intensity distributions at the focal plane (α) and far from it (β); the experimental interference spirals near the focal plane (γ) and far from it (δ).

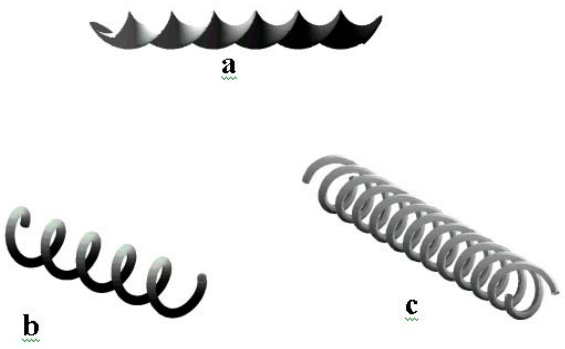

Fig. 14. Vortex preserving fibers: (a) the elliptical-twisted core; (b) the single spiral core; (c) the duel-spiral core.

Let us consider an optical fiber with the inner core wound around some axis in a spiral. (Fig. 14b). The Poynting vectors of all guided fiber modes are in the same whirl movement and eigenmodes obtain the same additional topological phase. The value of such a phase per one spiral turn may be found as it has been shown in Sec. III.1.3 and it equals

$$\Gamma_{sp} = 2\pi\left(1-\cos\chi\right), \qquad (3.28)$$

where the spiral torsion is defined by $\cos\chi = \frac{2\pi\Re}{\sqrt{(2\pi\Re)^2 + h^2}}$, $\Re$ - the spiral radius and h is the spiral pitch. At the distance z the topological phase will be $\Gamma_{tot} = N\Gamma_{sp}$, where the number of the spiral turns is $N \approx z/h$.

On the other hand, the Painting vector of the generic vortex in the straight fiber section accomplishes a proper precession movement. Besides, as it was mentioned above, the CV vortex, TE and TM modes gain different polarization corrections $\delta\beta_{prec}$ at the expense of their proper precessions. However, if the value of Berry's phase induced by the spiral core is larger then the proper Berry's phase per unit length for each mode $\frac{\Gamma_{tot}}{z} >> \delta\beta_{\max}^{(s-o)}$, then a synchronization event takes - place. It means that the nutation movement suppresses all other Poynting vector movements and imposes the new regime of the mode transmitting. In fact, all fiber-guided modes with close values of the propagation constant combine with each other forming four new wave states – the eigen guided vortices.

For simplicity one assumes that an optical fiber has the parabolic-index profile Then the polarization correction is [82]

$$\delta\beta_{\max}^{(s-o)} = \left|\frac{(2\Delta)^{\frac{3}{2}}}{2\rho V}(l+1)\right|, \qquad (3.29)$$

By combining eq.(3.26) and (3.27) one obtains the requirement of the fiber vortex preservation:

$$\frac{1}{4\pi}\frac{h}{z_0} + \frac{1}{\sqrt{1+\left(\frac{2\pi\Re}{h}\right)^2}} << 1, \quad z_0 = \frac{k\rho^2}{2}\, n_{co} \qquad (3.30)$$

The estimations show that dimensions of the spiral pitch and its radius have sufficiently rational values ($\Re \propto 20 \div 40\,\mu m$ and $h \propto 60 \div 100\,\mu m$) for the elaboration of the vortex preserving fibers. It should be noticed that such fibers may have also a twisting and duel-spiral core (Fig. 18b,c).

V. Conclusions

Singular Optics being one of the new branches of Modern Optics studies a wide class of electromagnetic phenomena associated with phase, polarization and amplitude singularities. Most of the authors characterize a vortex state in free space by means of only a topological charge while an optical vortex in a guiding system nevertheless needs two numbers – the topological charge l and helicity σ. It means that a vortex propagation in inhomogeneous media is hardly connected with its generic peculiarity – a polarization state. The coupling of the topological charge and helicity is of the spin – orbit interaction. It is the interchange between the spin and orbit characteristics in a singular beam that causes the splitting of the propagation constant levels in a fiber. Moreover,

the spin – orbit interaction stimulates an additional level splitting at the expense of external fiber perturbations. These conditions restrict a vortex lifelength constricting scope of the vortex applications in real fiber-optical devices. At the same time, use of a guided vortex even in customary low-mode optical fibers for optical sensors enlarges their sensitivity almost twice as much as the usual interferometric devices.

In our review we showed that there exist at least two ways of manufacturing vortex preserving fibers: either the fibers with absorption impurity centers doped near a fiber axis or the coiled-core ones. Such a fiber construction suppresses noise modes while the properties of a single fiber vortex almost are practically not affected.

Acknowledgements

The author is grateful to C.N. Alexeyev and T.A. Fadeyeva for helpful discussions, collaboration and the help in the paper design.

VI. References

1. Berry M. Singularities in waves and rays. In Physics of Defects, eds Balitan R., Kleman M. and Poirier J.-P. Noth-Holand, Amsterdam (1981). 457-538.
2. Nye J. F. Natural Focusing and Fine Structure of Light Caustics and Wave Dislocations. Institute of Physics Publishing, Bristol (1999).
3. Born M., Wolf E. Principles of Optics, 7th ed. Pergamon, New York, (1999).
4. Ignatovskii V.S. Trans. Opt. Inst., V.1, paper IV, Petrograd, (1919).
5. Richards B., Wolf E. Proc. R. Soc. London, Ser. A. **253** (1957) 358-370.
6. Wolf E. Proc. Symp. On Modern Optics, New York, No 2, (1969). 433-452.
7. Boivin A., Dow J., Wolf E. J. Opt. Soc Amer. **57(10)** (1967) 1171-1175.
8. Carter W. H. Opt. Commun. **7** (1973) 211-227.
9. Karman G.P., Beijersbergen M.W., van Duijl A., Bouwmeester D., Woerdman J.P. J. Opt. Soc. Amer. A, **15 (4)** (1998) 884-859.
10. Berry M.V. J. Mod. Opt. **45 (**1998**)** 1845-1851.
11. Nye J.F. J. Opt. Soc. Amer. A. **15(5)** (1998) 1132-1138.
12. Volyar A.V., Shvedov V.G, Fadeeva T.A. Optics and Spectroscopy. **90(1)** (2001) 93-100 (in Russian).
13. Volyar A.V., Shvedov V.G, Fadeeva T.A. Optics and Spectroscopy. **91(2)** (2001) 235-245 (in Russian).
14. Pas'ko V.A., Soskin M.S., Vasnetsov M.V. Opt. Commun. **198** (2001) 49-56.
15. Berry M.V., Chambers R.G., Large M.D., Upstill C., Walmsley J.C. Eur. J. Phys. **1** (1980) 154-162.
16. Berry M. J. Phys. A: Math. Gen. **32** (1999) 5627-5641.
17. Dirac P.A.M. Magnetic monopole. In Directions of Physics, eds. Hora, J. Shepanski, Jone Wiley and Sons, New York (1978)
18. Berry M.V. Proc. R. Soc. London A **392** (1984) 45-57. (See also in Geometric Phases in Physics eds. Shapere A. and Wilczek F. Advanced Ser. in Math. Phys., **5** (1989)).
19. Wright F.J. Proc. Int. Symposia on Applications of Catastrophe Theory and Topological Concepts in Physics. Tuebinen, Germany, May and December, Springer, Berlin (1978) 141-254.
20. Vasnetsov M.V., Staliunas K., eds. Optical Vortices. Nova Science Publishers, New York. (1999)
21. Kivshar Yu.S., Pelinovsky D.E. Phys. Rep. **331** (2000) 117-195.
22. Soskin M.S., Vasnetsov M.V. Progress in Optics 42, eds. Wolf E., Chapter 4, (2001) 219-276.
23. Allen L., Padgett M., Babiker M. Progress in Optics XXXIX. eds. Wolf E. (1999) 291-372.

24. Freund. I. Opt. Commun.**159** (1999) 99-117.
25. Weiss C.O., Vilaseca R. Dynamics of Lasers. Weinheim, New York. (1991).
26. Volyar A.V., Fadeyeva T.A. Optics and Spectroscopy. **85(2)** (1998) 264-271 (in Russian).
27. Volyar A.V., Fadeyeva T.A. Optics and Spectroscopy. **85(2)** (1998) 272-280 (in Russian).
28. Abramochkin E., Volostnikov V. Opt. Commun. **83 (1,2)** (1991) 123-135.
29. Abramochkin E., Losevsky N., Volostnikov V. Opt. Commun. **141** (1997) 59-64.
30. Haris M., Hill C.A., Vaughan J.M. Opt. Commun. **105** (1991) 161-166.
31. Tumbull G.A., Robertson D.A., Smith G.M., Allen L., Padgett M.J. Opt. Commun.**127** (1996) 183-188.
32. Izdebskaya Ya. V., Shvedov V.G., Kurabtzev D., Alexeyev A.N., Volyar A.V. Proc. of SPIE. **4607** (2001) 78-82.
33. Nye J.F., Berry M.V. Proc. R. Soc. Lond. A. **336** (1974) 165-190.
34. Sheppard C.J.R., Saghafi S. Phys. Rev. A, **57 (4)** (1998) 2971-2979.
35. Felson L.B. J. Opt. Soc. Amer. **66 (8)** (1976) 751-760.
36. Volyar A.V. Techn. Phys. J. Lett. **26(13)** (2000) 71-78.
37. Sigman A.E. J. Opt. Soc. Amer. **63 (9)** (1973) 1093-1094.
38. Kiselev A.P., Perel M. P. J. Math. Phys. **41 (4)** (2000) 1934-1955.
39. Volyar A.V., Shvedov V.G. Proc. of SPIE. **4403** (2000) 59-63.
40. Freund I. Proc. of SPIE. **4403** (2000) 24-35.
41. Allen L., Beijersbergen M.W., Spreeuw R.J.C., Woerdman J.P. Phys. Rev. A, **45 (11)** (1992) 8185-8189.
42. Barnet S.M., Allen L. Opt. Commun. **110** (1994) 670-678.
43. Volyar A.V., Fadeyeva T.A., Shvedov V.G. Techn. Phys. J. Lett. **25 (5)** (1999) 87-95 (in Russian).
44. Beth R.A. Phys. Rev. **50** (1936) 115-125.
45. Beijersbergen M.W., Allen L., van der Veen H.E.L.O., Woerdman J.P. Opt. Commun. **96** (1993) 123-132.
46. Courtial J., Padgett M.J. Opt. Commun. **159** (1999) 13-18.
47. O'Neil A.T., Courtial J. Opt. Commun.**181** (2000) 35-45.
48. Volyar A.V., Fadeyeva T.A., Shvedov V. G. J. Tech. Phys. Lett. **26 (22)** (1999) 14-20 (in Russian).
49. Terriza G.M., Recolons J., Torres J.P., Torner L. Phys. Rev. Lett. **87 (2)** (2001) 023902-1-023904.
50. Saks Z.S., Rozas D., Swartzlander G.A. J. Opt. Soc. Amer. B. **15 (8)** (1998) 2226-2234.
51. Bazhenov V.Yu., Vasnetsov M.V., Soskin M.S. JETP Lett. **52** (1990) 429-431 (in Russian).
52. Heckenberg N.R., McDuff R., White A.G. Opt. Lett. **17** (1992) 221-223.
53. Oran R., Davidson N., Friesem A.A., Hasman E. Opt. Commun. **182** (2000) 205-208.
54. Masajada J. Optik. **110 (12) (**1999) 554-558.
55. Alexeyev A.N., Borodavka O.S., Snvedov V.G. Proc. of SPIE. **3904 (**1999) 68-73.
56. Gorshkov N.V., Kononenco A.N., Soskin M.S. Proc. of SPIE. **4607** (2001) 13-24.
57. Shvedov V.G., Izdebskaya Ya. V., Alexeyev A.N., Volyar A.V. Techn. Phys. J. Lett. **28 (6)** (2002) 87-93 (in Russian).
58. Volyar A.V., Fadeyeva T.A., Shvedov V.G. J. Optics and Spectroscopy (in Russian) (to be published).
59. Azzam R.M.A., Bashara N.M. Ellipsometry and Polarized Light. Noth-Holland Publishing Company, Amsterdam, New York, Oxford. (1977).
60. Baranova N. B., Zel'dovich B.Ya., Mamaeyev A.V. JETP Lett. **33** (1981) 206-209 (in Russian).
61. Darsh M. Ya., Zel'dovich B.Ya., Kataeyevskaya I.V., Kundicova N.D. JETP, **107 (5)** (1995) 1464-1472 (in Russian).

62. Volyar A.V., Fadeyeva T.A. Techn. Phys. J. Lett. **22 (8)** (1996) 63-67 (in Russian).
63. Volyar A.V., Fadeyeva T.A. Techn. Phys. J. Lett., **22 (17)** (1996) P. 75-87 (in Russian).
64. Abramochkin E.G., Losevsky N.N., Volostnikov V.G. Proc. of SPIE. **4403** (2000) 189-191.
65. Balistreri M.L., Korterk J.P., Kuipers L., van Hulsi N.F. Phys. Rev. Lett., **85 (2)** (2000) 294-297.
66. Angelsky O.V., Besagha R.N., Mockun I.I. Optics and Spectroscopy. **82 (4)** (1997) 621-629 (in Russian).
67. Volyar A.V., Zhilaitis V.Z., Shvedov V.G. Optics and Spectroscopy. **86 (4)** (1999) 664-670 (in Russian).
68. Alexeyev C.N., Fridman Yu.A., Alexeyev A.N. Ukr. J. Phys. **40 (6)** (1999) 694-700.
69. Liberman V.S., Zel'dovich B.Ya. Phys. Rev. *A*. **45 (8)** (1992) 5199-5207.
70. Liberman V.S., Zel'dovich B.Ya. Phys. Rev. E. **49 (3)** (1994) 2389-2396.
71. Savchenko A.Yu., Zel'dovich B.Ya. Phys. Rev. E. **50 (3)** (1994) 2287-2262.
72. Volyar A.V., Fadeyeva T.A. Optics and Spectroscopy. **86 (2)** (1999) 242-250 (in Russian).
73. Alexeyev C.N., Fadeyeva T.A., Volyar A.V., Soskin M.S. Semiconductor Physics. Quantum Electronics & Optoelectronics. **1 (1)** (1998) 82-89.
74. Volyar A.V., Zhilaitis V.Z., Shvedov V.G., Soskin M.S., Fadeyeva T.A. Optics of Atmosphere and Ocean. **11 (11)** (1998) 1199-1214.
75. Alexeyev C.N., Fridman Yu.A., Alexeyev A.N. Ukr. J. Phys. **44 (1)** (2001) 43-51.
76. Mc Gloin D., Simpson N., Padget M. Applied Optics.**37** (1998) 469-471.
77. Alexeyev C.N., Alexeyev A.N., Fridman Yu.A. Proc. of SPIE. **3487** (1997) 94-100.
78. Alexeyev C.N., Soskin M.S., Volyar A.V. Semiconductor Physics. Quantum Electronics & Optoelectronics. **3 (4)** (2000) 500-513.
79. Alexeyev C.N., Volyar A.V. Proc. of SPIE. **4403** (2000) 170-176.
80. Alexeyev C.N., Volyar A.V. Proc. of SPIE. **4607** (2001) 71-77.
81. Volyar A.V., Fadeyeva T.A. Proc. of SPIE. **4607** (2001) 30-39.
82. Snyder A.W., Love J.D. Optical Waveguide Theory. Chapman and Hall, London, New York. (1983).
83. Yariv A., Yeh P. Optical Waves in Crystals. A Wiley-Interstice Publishing, John Wiley & Sons, New York. (1984).
84. Davidoff A.S. Quantum Mechanics. Moscow, Nauka. (1976). (in Russian).
85. Tomita A., Chiao R.Y. Phys. Rev. Lett. **57 (8)** (1986) 937-940.
86. Berry M.V. Nature. **326** (1987) 277-278.
87. Yeh C., Ha K., Dong S.B., Brown W.P. Appl. Opt. **18 (10)** (1979) 1490-1504.
88. Scherer G.W. Appl. Opt. **19 (12)** (1980) 2000-2006.
89. Shihata N., Okamoto K., Suzuki K., Ishida Yu. J. Opt. Soc. Amer.**73 (12)** (1983) 1792-1798.
90. Hughes R., Priest R. Appl. Opt. **19 (9)** (1979) 1477-1483.
91. Tateda M., Tanaka S., Sugawara Ya. Appl. Opt. **19 (5)** (1980) 770-773.
92. Fang X.-S., Lin Z.-Q. J. Lightwave Techn. **LT-3 (3)** (1985) 789-794.
93. Carrata S.L.A., Almeida S.F.M., Covingion C.E., Blake N. J. Opt. Soc. Amer. **12 (5)** (1995) 869-880.
94. Saijonmaa J., Vevick D. J. Opt. Soc. Amer. **73 (12)** (1983) 1785-1791.
95. Smith A.M. Appl. Opt. **19 (15)** (1980) 2606-2611.
96. McIntyre P., Snyder A. J. Soc. Amer. **68 (2)** (1978) 149-157.
97. Ulrich R., Simon A. Appl. Opt. **18 (13)** (1979) 2241-2251.
98. Sakai J.-I., Kimura T. J. Quant. Elect. **QE-17 (8)** (1981) 1842-1851.
99. Kaminov I.P., Ramaswamy V. Appl. Phys. Lett. **34** (1979) 268-270.

100. Alexeyev C.N., Volyar A. V., Fadeyeva T.A. Optics and Spectroscopy (in Russian) (to be published).
101. Savchenko A.Yu., Zel'dovich B. Ya. J. Opt. Soc. Amer. B. **13 (2)** (1996) 273-281.
102. Kusano K., Ankiewicz A., Burke S.V. Appl. Optics. **35 (12)** (1996) 2041-2047.
103. Verrier I., Goure J.P. Opt. Lett. **15 (1)** (1990) 15-17.
104. Marcuse D. Light Transmission Optics. Van Nostrand Rainhold Company, New York. (1972).
105. Eighman G. J. Opt. Soc. Amer. **61 (2)** (1971) 161-168.
106. He H., Friese M.E.J., Heckenberg N.R., Rubinsztein-Danlop H. Phys. Rev. Lett. **75 (5)** (1995) 826-829.
107. Volyar A.V., Fadeyeva T.A., Shvedov V.G. Proc. of SPIE. **4403** (2000) 153-161.
108. Egorov Yu.V., Alexeyev A.N., Shipulin O.A., Volyar A.V. Proc. of SPIE. **4607** (2001) 54-58.
109. Fadeyeva T.A., Kurabtzev D., Volyar A.V., Soskin M.S. Proc. of SPIE. **4607** (2001) 83-89.
110. Fadeyeva T.A., Volyar A.V., Reshetnickoff S.A., Alexeyev A.N. Proc. of SPIE. **4403** (2000) 307-311.
111. Volyar A.V., Fadeyeva T.A., Lapaeyeva S.N. Tech. Phys. J. Lett. **90 (1)** (2001) 30-37 (in Russian).
112. Volyar A.V., Fadeyeva T.A. Techn. Phys. J. Lett. **28 (3)** (2002) 42-48 (in Russian).
113. Barlow A.J., Ramskov-Hansen J.J., Payne D.N. Appl. Opt. **20 (17)** (1981) 2962-2968.
114. Fujil Yo., Sano K. Appl. Opt. **19 (15)** (1980) 2602-2605.
115. Shibana N., Tsubokawa M., Seikai Sh. Opt. Lett.**16 (2)** (1985) 92-94.
116. Mayastre F., Bertholds A. Opt. Lett. **14 (11)** (1989) 587-589